AIMS Mathematics, 11(5): 13339–13370.
DOI: 10.3934/math.2026550
Received: 25 February 2026
Revised: 26 April 2026
Accepted: 08 May 2026
Published: 13 May 2026

http://www.aimspress.com/journal/Math

Research article

Modeling tuberculosis transmission dynamics in Algeria: Effects of vaccination, exogenous reinfection, and endogenous reactivation

Rayane Boucherma[1,2], Mohammed-Salah Abdelouahab[2,3], Messaoud Berkal[2,3], Taha Radwan[4,*], Yakup Yildirim[5,6] and Karim K. Ahmed[7]

[1] Laboratoire des Mathématiques Appliquées et Didactique, Ecole Normale Supérieure de Constantine, Constantine, Algeria
[2] Department of Mathematics and Computer Sciences, University Abdelhafid Boussouf, Mila 43000, Algeria
[3] Laboratory of Mathematics and Their Interactions, Abdelhafid Boussouf University, Mila 43000, Algeria
[4] Department of Management Information Systems, College of Business and Economics, Qassim University, Buraydah 51452, Saudi Arabia
[5] Department of Computer Engineering, Biruni University, Istanbul 34010, Turkey
[6] Mathematics Research Center, Near East University, Nicosia 99138, Cyprus
[7] Department of Mathematics, Faculty of Engineering, German International University (GIU), New Administrative Capital, Cairo, Egypt

* **Correspondence:** Email: t.radwan@qu.edu.sa.

Abstract: This paper developed a novel nonlinear Susceptible–Vaccinated–Exposed–Infectious–Treated–Recovered–Susceptible (SVEITRS) compartmental model to investigate the transmission dynamics of tuberculosis (TB) in Algeria over the period between 1990–2024, explicitly accounting for partial Bacillus Calmette-Guérin (BCG) vaccine efficacy, endogenous reactivation of latent infection, and exogenous reinfection. The basic reproduction number $\mathcal{R}_0$ was derived using the next-generation matrix approach, and rigorous analytical results were established for the local and global stability of both the disease-free and endemic equilibrium points. Model parameters were estimated by fitting the model to Algerian TB surveillance data, achieving a coefficient of determination of $R^2 = 0.84$, which indicates a strong agreement between the model predictions and reported epidemiological trends. A global sensitivity analysis based on partial rank correlation coefficients (PRCCs) reveals that demographic recruitment and transmission-related parameters exert the greatest influence on TB dynamics, whereas intervention-related parameters such as vaccination and treatment rates have a comparatively weaker impact. These findings indicate that vaccination alone is insufficient to eliminate TB and highlight the need for integrated control strategies that combine sustained vaccination coverage,

early case detection, and effective management of latent infections. The proposed modeling framework provides a quantitative basis for evaluating TB control policies in high-burden settings such as Algeria.

Keywords: mathematical model; tuberculosis; endogenous reactivation; exogenous reinfection; parameter estimation; partial rank correlation coefficient (PRCC)
Mathematics Subject Classification: 34A55, 92D30, 62F10

1. Introduction

Tuberculosis (TB), caused by *Mycobacterium tuberculosis (Mtb)*, remains a major global public health challenge. Although TB primarily affects the lungs, Mtb can disseminate to other organs, resulting in extrapulmonary TB, which is generally noncontagious [1, 2]. Clinically, active TB is characterized by persistent cough, chest pain, fever, weight loss, and night sweats [3], and it is transmitted through airborne droplets expelled by infectious individuals. Following infection, most individuals develop latent TB, with an estimated lifetime risk of approximately 10% for progression to active disease [4]. Notably, coinfection with HIV/AIDS substantially increases the risk of latent TB reactivation.

The treatment of active TB requires prolonged antibiotic regimens to reduce the risk of relapse, although complete cure is not always guaranteed. In the absence of treatment, active TB is associated with a mortality rate exceeding 50% and may lead to severe complications, particularly among pregnant women, including low birth weight [5]. The emergence of drug-resistant TB strains has further complicated disease management. Meanwhile, the Bacille–Calmette–Guérin (BCG) vaccine confers only partial and time-limited protection, typically lasting 10–15 years [6, 7]. Although the introduction of antibiotics such as streptomycin and isoniazid initially raised optimism regarding TB eradication, the combined challenges of antimicrobial resistance and the HIV/AIDS epidemic have necessitated intensified global control efforts, particularly in resource-limited settings [1].

The complexity and heterogeneity of infectious disease transmission at the population level highlight the critical role of mathematical modeling in evaluating intervention strategies [8–10]. Such models have become indispensable for understanding TB dynamics and assessing the potential impact of control measures. Previous studies have employed a wide range of modeling frameworks, including epidemiological models, integer time-series approaches, and compartmental models [11–13]. Despite these advances, there remains a pressing need for more comprehensive, data-driven models capable of integrating multiple intervention strategies.

To bridge these gaps, numerous studies have investigated TB transmission dynamics across diverse settings. For instance, Liu et al. [14] examined seasonal variations in TB incidence using epidemiological data for parameter estimation. Other research has focused on high-burden regions, such as the Asia-Pacific [15] area, and has explored intervention strategies in China, including relapse dynamics [16, 17]. Compartmental modeling approaches have also been applied to TB dynamics in Algeria [18] and jointly in Algeria and Ukraine [19,20], with an emphasis on vaccination and treatment strategies. Additionally, discrete-time models incorporating chemoprophylaxis have been developed to study multidrug-resistant (MDR) and extensively drug-resistant (XDR) TB in countries such as Russia and India [21].

For example, Joshi and Yavuz [22] analyzed the interaction between COVID-19 and TB dynamics, highlighting the impact of coexisting epidemics on disease transmission. In a related context, Peter et al. [23] employed simulation-based approaches to optimize TB control strategies. Similar optimization frameworks have also been successfully applied to other infectious diseases, including measles [24], demonstrating the versatility of such methodologies across different epidemiological settings.

In addition, Yavuz et al. [25] investigated the role of public awareness campaigns in mitigating disease spread, while Bolaji et al. [26] examined the dynamics of HIV–TB coinfection. Other studies have further incorporated behavioral responses and awareness-driven mechanisms into epidemiological models [27], as well as combined vaccination and treatment strategies [28].

Furthermore, more advanced modeling approaches, such as patch-based epidemic frameworks [29], and data-driven applications based on real-world datasets, including hepatitis B modeling [30], highlight the growing importance of integrating realistic data and spatial heterogeneity into infectious disease modeling.

A crucial aspect of TB transmission dynamics is the interplay between endogenous reactivation in latent or recovered individuals and exogenous reinfection due to contact with infectious cases. Incorporating both mechanisms into mathematical models enhances their realism, and reducing their respective rates, in combination with vaccination, can significantly lower TB prevalence [31].

Algeria provides a pertinent case study for TB transmission modeling due to its sustained disease burden and heterogeneous epidemiological landscape. According to the World Health Organization, approximately 19,000 new TB cases were reported in 2021, of which about 1.4% were classified as multidrug-resistant TB (MDR-TB) [32]. Transmission patterns are shaped by pronounced spatial heterogeneity, ranging from densely populated urban centers to remote areas with limited access to healthcare services.

From a demographic perspective, Algeria exhibits a relatively high life expectancy (77.1 years in 2020), ranking 51st globally [33]. This demographic profile may amplify the role of latent infection, endogenous reactivation, and exogenous reinfection in maintaining TB transmission. In this context, the present study calibrates a mechanistic TB model using Algerian data to evaluate control strategies under these complex epidemiological conditions.

The present work focuses on clinically active TB as the primary driver of transmission, given its well-established dominant role in disease spread. This assumption facilitates analytical tractability and aligns with epidemiological evidence highlighting the central contribution of symptomatic individuals.

Nevertheless, transmission may also occur during a subclinical stage (distinct from latent infection), where asymptomatic individuals remain infectious, albeit at a lower per-contact rate than clinically active cases. Such subclinical forms have been reported in high-burden settings, where delayed detection may prolong their infectious period.

Recent modeling efforts, including the discrete-time model by Ripoll and Font [34], have addressed infection dynamics prior to symptom onset. The present model captures the principal transmission pathway through clinically active TB. The explicit inclusion of subclinical transmission will be a direction for our future work.

Building on our previous work [20], this study introduces a six-dimensional SVEITRS model to better capture the complex dynamics of tuberculosis. The model explicitly accounts for latent infection, endogenous reactivation, exogenous reinfection, vaccination, and waning post-treatment immunity, allowing recovered individuals to return to the susceptible class. By integrating these mechanisms, the

model provides a realistic representation of TB transmission and progression. This high-dimensional framework enables the analysis of the combined effects of vaccination strategies, reinfection, and reactivation on disease dynamics, offering deeper epidemiological insights and actionable guidance for public health interventions. Importantly, it successfully reproduces the non-monotonic trends observed in historical data from 1990 to 2024, ensuring a superior fit compared to lower-dimensional models and supporting robust long-term forecasts until 2050.

2. Mathematical model

In this study, we develop a deterministic epidemiological model to investigate the transmission dynamics of tuberculosis (TB) in Algeria over the period between 1990–2024. The total population $N(t)$ is partitioned into six epidemiological compartments: Susceptible (S), Vaccinated (V), Exposed (E), Infectious (I), Treated (T), and Recovered (R). Natural mortality is assumed to occur in all compartments at a constant rate μ.

The dynamics of the susceptible population $S(t)$ are driven by the recruitment of newborns who do not receive the BCG vaccine, represented by the term $(1-\rho)\lambda$, where $0 < \rho < 1$ denotes the vaccination coverage at birth. This class is further augmented by individuals who lose their immunity and return to the susceptible state; this includes vaccinated individuals whose vaccine-induced protection wanes at a rate k, and recovered individuals whose infection-acquired immunity wanes at a rate ϕ. Conversely, the susceptible population is depleted by natural death at a rate μ and by effective contact with infectious TB cases at a transmission rate β.

The vaccinated compartment $V(t)$ consists of individuals immunized at birth at a rate $\rho\lambda$. Although the BCG vaccine provides partial protection against TB, its effectiveness diminishes over time, leading vaccinated individuals to return to the susceptible class at a rate k. Moreover, due to imperfect vaccine efficacy, vaccinated individuals may still acquire infection upon exposure to infectious cases. This phenomenon is modeled by the parameter ξ, which represents vaccine failure. Natural mortality also affects this compartment at a rate μ.

The exposed compartment $E(t)$ represents individuals with latent TB infection. This class receives individuals through three primary pathways: Infection of susceptible individuals, breakthrough infection among vaccinated individuals due to vaccine failure, and exogenous reinfection of recovered individuals, governed by the parameter θ. This latter mechanism captures repeated exposure to infectious cases in high-risk environments. Additionally, endogenous reactivation of latent infection during treatment occurs at a rate δ, where a fraction $(1-p)$ of such individuals returns to the exposed class. Individuals in this compartment progress to active TB at a rate ϵ.

The infectious compartment $I(t)$ comprises individuals with active and transmissible TB. Inflows into this class arise from the progression of latent infection at a rate ϵ, as well as from endogenous reactivation during treatment, where a fraction p of reactivated individuals develops active TB. Individuals leave this compartment either by initiating treatment at a rate γ or through disease-induced mortality at a rate η.

The treated compartment $T(t)$ comprises individuals receiving therapy. While successful treatment leads to recovery at a rate σ, relapse or reactivation may force individuals back to infected or exposed states. Notably, treatment is assumed to reduce TB-related mortality by approximately 50% ($\eta/2$). This parameterization is justified by clinical evidence regarding the natural history of the disease; for

instance, untreated pulmonary tuberculosis in HIV-negative patients has a weighted mean 10-year case fatality rate of approximately 70% [35]. Given that modern chemotherapy can reduce this risk to minimal levels in clinical settings, our assumption of a 50% reduction ($\eta/2$) represents a realistic and conservative estimate that accounts for population-level challenges such as treatment adherence and healthcare access. This approach remains consistent with the Stop TB Partnership targets integrated into Algeria's national tuberculosis strategy [32].

The recovered compartment $R(t)$ consists of individuals who have successfully completed treatment and acquired temporary immunity. This immunity is not permanent and wanes over time, causing individuals to revert to the susceptible class at a rate ϕ. Additionally, individuals in this compartment are subject to natural mortality at a rate μ.

The transmission dynamics of the integer TB model are

$$\begin{cases} \dfrac{dS}{dt} = (1-\rho)\lambda + kV(t) + \phi R(t) - \beta S(t)I(t) - \mu S(t), \\ \dfrac{dV}{dt} = \rho\lambda - (k+\mu)V(t) - \xi V(t)I(t), \\ \dfrac{dE}{dt} = \xi V(t)I(t) + \beta S(t)I(t) + \theta\beta R(t)I(t) - (\epsilon+\mu)E(t) + (1-p)\delta T(t), \\ \dfrac{dI}{dt} = \epsilon E(t) + p\delta T(t) - (\mu+\eta+\gamma)I(t), \\ \dfrac{dT}{dt} = \gamma I(t) - (\delta+\sigma+\mu+\eta/2)T(t), \\ \dfrac{dR}{dt} = \sigma T(t) - (\mu+\phi)R(t) - \theta\beta R(t)I(t). \end{cases} \tag{2.1}$$

The initial conditions for the model are defined as follows:

$$S(0) = S_0, \quad V(0) = V_0, \quad E(0) = E_0, \quad I(0) = I_0, \quad T(0) = T_0, \quad R(0) = R_0,$$

where the total population at any time t is given by:

$$N(t) = S(t) + V(t) + E(t) + I(t) + T(t) + R(t).$$

All parameters are summarized and biologically interpreted in Table 1. The structure of the model is illustrated in Figure 1.

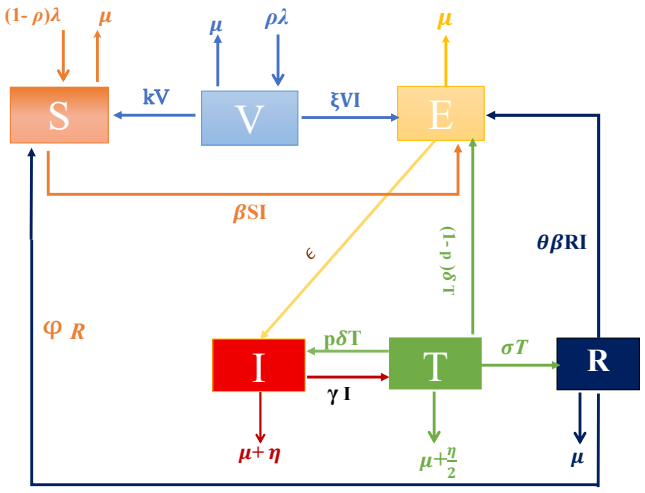

Figure 1. Flowchart of the SVEITRS model. The six compartments, Susceptible (S), Vaccinated (V), Exposed (E), Infected (I), Treated (T), and Recovered (R), and their key transitions are illustrated. These include recruitment (λ), infection (β, ξ, θ), progression (ϵ), treatment and recovery (γ, σ), waning immunity (k, ϕ), reactivation (δ), and mortality (μ, η).

Table 1. Model variables, parameters, and their descriptions.

Variables and parameters	**Description**
$S(t)$	Number of susceptible individuals who can become infected at time t.
$V(t)$	Number of vaccinated individuals at time t.
$E(t)$	Number of exposed individuals at time t.
$I(t)$	Number of infected individuals at time t.
$T(t)$	Number of individuals undergoing treatment at time t.
$R(t)$	Number of recovered individuals at time t.
λ	Recruitment rate.
β	Transmission rate.
k	Waning rate of vaccine-induced immunity.
ρ	Vaccination rate.
ξ	Rate of vaccine failure leading to exposure.
ϵ	Development rate from exposed E to infected I.
ϕ	Rate of loss of immunity in recovered individuals.
δ	Endogenous reactivation rate of dormant infection within the T class.
θ	Exogenous reinfection coefficient.
γ	Rate of treatment of the non-isolated infected class.
σ	Rate of recovery from treated T to recovered R.
p	Fraction of treatment failure leading to active TB.
μ	Natural death rate.
η	TB-related death rate in the infected population I.
$\eta/2$	TB-related death rate in the treated population T.

3. Dynamical analysis

3.1. Invariance of the feasible region

Lemma 3.1. *(Positivity and boundedness) For all $t > 0$ and non-negative initial conditions, the solution of the TB model* (2.1) *is positive whenever it exists.*
Furthermore, if $0 \leq N(0) \leq \dfrac{\lambda}{\mu}$, *then* $0 \leq N(t) \leq \dfrac{\lambda}{\mu}$ *for all* $t > 0$.

Proof. We first define the biologically feasible region:

$$\Pi = \left\{(S, V, E, I, T, R) \in \mathbb{R}^6_+ : N(t) \leq \frac{\lambda}{\mu}\right\}, \tag{3.1}$$

where $N(t) = S(t) + V(t) + E(t) + I(t) + T(t) + R(t)$.
To prove the positivity of the solution, we consider the system $\dot{x} = f(x)$, where $x = (S, V, E, I, T, R)^T$. For each component x_i, the solution remains non-negative if $f_i(x) \geq 0$ whenever $x_i = 0$ and all other components $x_j \geq 0$ for $j \neq i$. From the system (2.1), we evaluate the derivatives on the boundaries of the non-negative orthant $\mathbb{R}^6_+$:

$$\begin{cases} \left.\dfrac{dS}{dt}\right|_{S=0} = (1-\rho)\lambda + kV + \phi R \geq 0, \quad for \;\; V, R \geq 0, \\ \left.\dfrac{dV}{dt}\right|_{V=0} = \rho\lambda \geq 0, \\ \left.\dfrac{dE}{dt}\right|_{E=0} = \xi VI + \beta SI + \theta\beta RI + (1-p)\delta T \geq 0, \quad for \;\; V, S, R, I, T \geq 0, \\ \left.\dfrac{dI}{dt}\right|_{I=0} = \epsilon E + p\delta T \geq 0, \quad for \;\; E, T \geq 0, \\ \left.\dfrac{dT}{dt}\right|_{T=0} = \gamma I \geq 0, \quad for \;\; I \geq 0, \\ \left.\dfrac{dR}{dt}\right|_{R=0} = \sigma T \geq 0, \quad for \;\; T \geq 0. \end{cases} \tag{3.2}$$

To complete the proof, we use the first time of exit argument. Let the initial conditions lie in the non-negative orthant, $x(0) \in \mathbb{R}^6_+$. Assume, for the sake of contradiction, that the solution $x(t)$ leaves this region. By the continuity of the solution, there exists a first time $t^* > 0$ defined as:

$$t^* = \inf\{t > 0 : x(t) \notin \mathbb{R}^6_+\}.$$

By the definitions of t^* and continuity, all components satisfy $x_j(t) \geq 0$ for $t \in [0, t^*)$, and at t^*, at least one component reaches the boundary, i.e., $x_i(t^*) = 0$ for some $i \in \{S, V, E, I, T, R\}$, while the remaining components remain non-negative due to the definition of t^*.

Evaluating the system at t^*, the expressions in (3.2) show that the derivative $\dot{x}_i(t^*)$ depends only on state variables that are non-negative at this instant. Hence, for any vanishing component $x_i(t^*) = 0$,

we obtain $f_i(x(t^*)) \geq 0$. This implies that the vector field on the boundary of $\mathbb{R}^6_+$ is either tangent to or directed toward its interior.

Therefore, the trajectory cannot cross into the negative region, and any solution starting in $\mathbb{R}^6_+$ remains in this region for all $t \geq 0$.

Consequently, $\mathbb{R}^6_+$ is a positively invariant set for system (2.1).

Regarding boundedness, we sum the equations of the system to obtain the rate of change of the total population $N(t)$:

$$\frac{dN}{dt} = \lambda - \mu N - [(\eta/2)T + \eta I] \leq \lambda - \mu N,$$

where $[(\eta/2)T + \eta I] \geq 0$ is the disease-induced death rate.

Moreover, since all compartments are initially non-negative,

$$S(0), V(0), E(0), I(0), T(0), R(0) \geq 0.$$

We have

$$N(0) \geq 0 \quad \Rightarrow \quad N(t) \geq 0 \quad \text{for all } t \geq 0.$$

From the Gronwall's inequality (or the comparison principle),

$$N(t) \leq N(0)e^{-\mu t} + \frac{\lambda}{\mu}(1 - e^{-\mu t}),$$

and it follows that

$$\lim_{t\to\infty} \sup N(t) \leq \frac{\lambda}{\mu}.$$

Moreover, if $N(0) \leq \dfrac{\lambda}{\mu}$, then

$$N(t) \leq \frac{\lambda}{\mu}, \quad \forall t \geq 0,$$

since the right-hand side is a convex combination of $N(0)$ and $\frac{\lambda}{\mu}$. Therefore, combining the lower and upper bounds, we obtain

$$0 \leq N(t) \leq \frac{\lambda}{\mu}, \quad \forall t \geq 0.$$

This shows that the total population is bounded and remains non-negative for all $t \geq 0$, confirming that the feasible region Π is positively invariant.

Remark. Although the above analysis holds for any initial condition $N(0) \geq 0$, the case $N(0) = 0$ corresponds to an initially empty population, which is not epidemiologically meaningful. However, from a mathematical standpoint, the model remains well-defined since

$$\left.\frac{dN}{dt}\right|_{N=0} = \lambda > 0,$$

implying that $N(t) > 0$ for all $t > 0$. Therefore, while the invariant region Π is valid for all $N(0) \geq 0$, we assume $N(0) > 0$ in practical applications to ensure biological relevance. □

3.2. Equilibrium solutions

The equilibrium solutions of the system (2.1) are obtained by setting all derivatives equal to zero.

1. **Disease-free equilibrium (DFE):**
   The DFE is given by:

$$\mathcal{E}_1 = (S_1^*, V_1^*, E_1^*, I_1^*, T_1^*, R_1^*) = \left(\frac{k\lambda\rho + (1-\rho)\lambda(k+\mu)}{\mu(k+\mu)}, \frac{\lambda\rho}{(k+\mu)}, 0, 0, 0, 0\right).$$

2. **Endemic equilibrium (EE):**
   The endemic equilibrium $\mathcal{E}_2 = (S_2^*, V_2^*, E_2^*, I_2^*, T_2^*, R_2^*)$ is the solution to the system where all derivatives are zero, with $I_2^* > 0$.
   Equilibrium equations set to zero:

$$\begin{aligned}
0 &= (1-\rho)\lambda + kV_2^* + \phi R_2^* - \beta S_2^* I_2^* - \mu S_2^*,\\
0 &= \rho\lambda - (k+\mu)V_2^* - \xi V_2^* I_2^*,\\
0 &= \xi V_2^* I_2^* + \beta S_2^* I_2^* + \theta\beta R_2^* I_2^* - (\epsilon+\mu)E_2^* + (1-p)\delta T_2^*,\\
0 &= \epsilon E_2^* + p\delta T_2^* - (\mu+\eta+\gamma)I_2^*,\\
0 &= \gamma I_2^* - (\delta+\sigma+\mu+\eta/2)T_2^*,\\
0 &= \sigma T_2^* - (\mu+\phi)R_2^* - \theta\beta R_2^* I_2^*.
\end{aligned}$$

   Solution structure in terms of I^*:

$$\begin{aligned}
S_2^* &= \frac{(1-\rho)\lambda + kV_2^* + \phi R_2^*}{\mu + \beta I_2^*},\\
V_2^* &= \frac{\rho\lambda}{k+\mu+\xi I_2^*},\\
T_2^* &= \left(\frac{\gamma}{\delta+\sigma+\mu+\eta/2}\right) I_2^* = b_1 I_2^*,\\
R_2^* &= \frac{\sigma T_2^*}{\mu+\phi+\theta\beta I_2^*},\\
E_2^* &= \left(\frac{(\mu+\eta+\gamma)I_2^* - p\delta T_2^*}{\epsilon}\right) = \left(\frac{b_2 I_2^* - p\delta T_2^*}{\epsilon}\right).
\end{aligned} \tag{3.3}$$

   Substituting the expressions of $S_2^*, V_2^*, E_2^*, R_2^*$, and T_2^* into the remaining algebraic equation of the system leads to a single equation in terms of I_2^*, which can be written as the following cubic polynomial:

$$P(I_2^*) = A_1(I_2^*)^3 + A_2(I_2^*)^2 + A_3 I_2^* + A_4 = 0. \tag{3.4}$$

The coefficients are given by:

$$A_1 = \beta^2\xi\theta\Big((1-p)\delta X_1 + \frac{\epsilon+\mu}{\epsilon}(p\delta X_1 + X)\Big),$$

$$A_2 = \theta\beta^2(\rho\lambda + \sigma X_1) + (1-p)\beta\delta X_1 + \frac{\epsilon+\mu}{\epsilon}(p\delta X + X_1)\beta(\xi(\mu+\phi) + \theta\beta((k+\mu)+\theta\mu)),$$

$$A_3 = \rho\lambda\beta(\mu+\phi+\mu\phi) + \theta\beta\sigma b_1(\beta(k+\mu)+\mu\xi) + \frac{\epsilon+\mu}{\epsilon}(p\delta X_1 + X)\beta((k+\mu)+\theta\mu) + \mu\xi(\mu+\phi)$$
$$+ \theta\lambda\beta^2(1-\rho)(k+\mu) + \beta\lambda\xi(1-\rho)(\mu+\phi),$$

$$A_4 = \frac{\Big(\rho\lambda((\mu+\phi)+\beta k) + (k+\mu)\Big(\theta\beta\sigma X_1 + (\mu+\phi)((1-p)\delta X_1 + \frac{\epsilon+\mu}{\epsilon}(p\delta X_1 + X) + \beta\lambda(1-\rho))\Big)\Big)\mu^2(k+\mu)d_2}{\mu(k+\mu)d_2 - \epsilon(\delta+\sigma+\mu+\frac{\eta}{2})(\xi\rho\lambda\mu + \beta\lambda(k+\mu(1-\rho)))}$$
$$\times (1-\mathcal{R}_0),$$

where

$$X = \mu+\eta+\gamma, \quad X_1 = \frac{\gamma}{\delta+\sigma+\mu+\eta/2}.$$

Since all model parameters are positive, it follows that $A_1 > 0$, $A_2 > 0$, and $A_3 > 0$, whereas the sign of A_4 depends exclusively on the value of the basic reproduction number $\mathcal{R}_0$.

If $\mathcal{R}_0 > 1$, then $A_4 < 0$, implying that the sequence of coefficients of $P(I_2^*)$ contains exactly one sign change. According to Descartes' Rule of Signs, this ensures the existence of a unique positive real root. Therefore, the system admits a unique endemic equilibrium point.

Conversely, if $\mathcal{R}_0 < 1$, then $A_4 > 0$, and all coefficients of the polynomial $P(I_2^*)$ are strictly positive. In this case, no sign changes occur in the sequence of coefficients. By Descartes' Rule of Signs, the polynomial has no positive real roots. Hence, no biologically meaningful endemic fixed point exists, and the disease-free equilibrium remains the only equilibrium state of the system.

3.3. The basic reproduction number ($\mathcal{R}_0$)

The basic reproduction number $\mathcal{R}_0$ is a threshold parameter that determines whether an infection can invade and persist in a population. It is computed using the next-generation matrix method [36,37]. To apply this method, we identify the infected compartments as $x = (E, I, T)^T$. The rate of appearance of new infections in the infected compartments, denoted by the vector function f, and the rate of transfer of individuals between these compartments, denoted by v, are given by

$$f(x) = \begin{bmatrix} \xi VI + \beta S I + \theta\beta RI \\ 0 \\ 0 \end{bmatrix}, \quad v(x) = \begin{bmatrix} (\epsilon+\mu)E - (1-p)\delta T \\ (\mu+\eta+\gamma)I - \epsilon E - p\delta T \\ (\delta+\sigma+\mu+\eta/2)T - \gamma I \end{bmatrix}.$$

The Jacobian matrices $\mathcal{F}$ and $\mathcal{V}$ are obtained by linearizing the system around the disease-free equilibrium (DFE), $E_1 = (S^*, V^*, 0, 0, 0, 0)$.

$$\mathcal{F} = \left[\frac{\partial f_i}{\partial x_j}(E_1)\right] = \begin{bmatrix} 0 & \frac{d_1}{\mu(k+\mu)} & 0 \\ 0 & 0 & 0 \\ 0 & 0 & 0 \end{bmatrix}, \quad \mathcal{V} = \left[\frac{\partial v_i}{\partial x_j}(E_1)\right] = \begin{bmatrix} \epsilon+\mu & 0 & -(1-p)\delta \\ -\epsilon & \mu+\eta+\gamma & -p\delta \\ 0 & -\gamma & \delta+\sigma+\mu+\eta/2 \end{bmatrix}.$$

Here, $d_1 = \xi\rho\lambda\mu + \beta\lambda(k + \mu(1-\rho))$, which is strictly positive for $0 \le \rho \le 1$.
The inverse of $\mathcal{V}$ is given by

$$\mathcal{V}^{-1} = \frac{1}{d_2}\begin{bmatrix} (\mu+\eta+\gamma)(\delta+\sigma+\mu+\eta/2) - p\delta\gamma & \gamma(1-p)\delta & (1-p)\delta(\mu+\eta+\gamma) \\ \epsilon(\delta+\sigma+\mu+\eta/2) & (\epsilon+\mu)(\delta+\sigma+\mu+\eta/2) & (1-p)\delta\epsilon + (\epsilon+\mu)p\delta \\ \epsilon\gamma & \gamma(\epsilon+\mu) & (\epsilon+\mu)(\mu+\eta+\gamma) \end{bmatrix},$$

where

$$d_2 = (\epsilon+\mu)(\mu+\eta+\gamma)(\delta+\sigma+\mu+\eta/2) - (1-p)\delta\gamma\epsilon - p\delta\gamma(\epsilon+\mu).$$

The positivity of d_2 plays a crucial role in ensuring the well-posedness of the model. Since all transition rates $(\epsilon, \mu, \eta, \gamma, \delta, \sigma)$ are strictly positive and $0 \le p \le 1$, it follows that

$$d_2 > (\epsilon+\mu)\left((\mu+\eta+\gamma)(\delta+\sigma+\mu+\eta/2) - \delta\gamma\right).$$

By expanding and simplifying, we obtain the following:

$$d_2 > (\epsilon+\mu)\left((\mu+\eta+\gamma)(\sigma+\mu+\eta/2) + (\mu+\eta)\delta\right) > 0.$$

Therefore, d_2 remains strictly positive for all biologically admissible parameter values.

The next-generation matrix is given by $\mathcal{F}\mathcal{V}^{-1}$, which takes the form

$$\mathcal{F}\mathcal{V}^{-1} = \frac{d_1}{d_2}\begin{bmatrix} \dfrac{\epsilon(\delta+\sigma+\mu+\eta/2)}{\mu(k+\mu)} & \dfrac{\epsilon(\epsilon+\mu)(\delta+\sigma+\mu+\eta/2)}{\mu(k+\mu)} & \dfrac{(1-p)\delta\epsilon + (\epsilon+\mu)p\delta}{\mu(k+\mu)} \\ 0 & 0 & 0 \\ 0 & 0 & 0 \end{bmatrix}.$$

The basic reproduction number $\mathcal{R}_0$ is then determined as the spectral radius of $\mathcal{F}\mathcal{V}^{-1}$, yielding

$$\mathcal{R}_0 = \frac{\epsilon(\delta+\sigma+\mu+\eta/2)d_1}{\mu(k+\mu)d_2}.$$

3.4. Stability analysis

3.4.1. Local stability analysis of the DFE

Theorem 3.2. *The disease-free equilibrium $\mathcal{E}_1$ of system (1) is locally asymptotically stable if $\mathcal{R}_0 < 1$, and unstable if $\mathcal{R}_0 > 1$.*

Proof. Evaluating the Jacobian matrix at $\mathcal{E}_1$, we obtain

$$J_{\mathcal{E}_1} = \begin{bmatrix} -\mu & k & 0 & -\beta S_1^* & 0 & 0 \\ 0 & -(k+\mu) & 0 & -\xi V_1^* & 0 & 0 \\ 0 & 0 & -(\epsilon+\mu) & \beta S_1^* & (1-p)\delta & 0 \\ 0 & 0 & \epsilon & -(\mu+\eta+\gamma) & p\delta & 0 \\ 0 & 0 & 0 & \gamma & -(\delta+\sigma+\mu+\eta/2) & 0 \\ 0 & 0 & 0 & 0 & \sigma & -(\mu+\phi) \end{bmatrix}.$$

The associated characteristic polynomial which is

$$P(\Lambda) = -(\mu + \Lambda)(k + \mu + \Lambda)(\mu + \phi + \Lambda)\left[\Lambda^3 + a_1\Lambda^2 + a_2\Lambda + a_3\right].$$

Equivalently,

$$P(\Lambda) = -(k + \mu + \Lambda)(\mu + \Lambda)(\mu + \phi + \Lambda)Q(\lambda),$$

where $Q(\Lambda) = \Lambda^3 + a_1\Lambda^2 + a_2\Lambda + a_3$, with coefficients

$$\begin{aligned}
a_1 &= 3\mu + \epsilon + \frac{3\eta}{2} + \gamma + \delta + \sigma,\\
a_2 &= (\epsilon + \mu)(\mu + \eta + \gamma) + (\epsilon + \mu)(\delta + \sigma + \mu + \eta/2)\\
&\quad + (\mu + \eta + \gamma)(\delta + \sigma + \mu + \eta/2) - \epsilon(\xi V_1^* + \beta S_1^*) - p\delta\gamma,\\
a_3 &= d_2(1 - \mathcal{R}_0), \qquad d_2 > 0.
\end{aligned}$$

The three explicit eigenvalues $-\mu$, $-(k + \mu)$, $-(\mu + \phi)$ are negative. The remaining eigenvalues are the roots of $Q(\Lambda)$.
The Routh–Hurwitz conditions for all roots of $Q(\Lambda)$ to have negative real parts are

$$a_1 > 0, \quad a_3 > 0, \quad a_1a_2 - a_3 > 0.$$

Clearly $a_1 > 0$. From $\mathcal{R}_0 < 1$, we obtain $a_3 = d_2(1 - \mathcal{R}_0) > 0$. It remains to prove $a_1a_2 - a_3 > 0$ under $\mathcal{R}_0 < 1$. We introduce the shorthand notations

$$X = \mu + \eta + \gamma, \quad Y = \delta + \sigma + \mu + \frac{\eta}{2}, \quad Z = \epsilon + \mu,$$

$$A = XY + YZ + ZX, \qquad d_2 = XYZ - \delta\gamma(\epsilon + p\mu) > 0.$$

Then one verifies that

$$a_1 = X + Y + Z, \qquad a_2 = A - p\delta\gamma - \frac{d_2}{Y}\mathcal{R}_0.$$

We define $\Delta = A - p\delta\gamma - \dfrac{d_2}{Y}$. Consequently

$$a_2 = \Delta + \frac{d_2}{Y}(1 - \mathcal{R}_0).$$

Now we compute

$$\begin{aligned}
a_1a_2 - a_3 &= a_1\Big[\Delta + \frac{d_2}{Y}(1 - \mathcal{R}_0)\Big] - d_2(1 - \mathcal{R}_0)\\
&= a_1\Delta + d_2\Big(\frac{a_1}{Y} - 1\Big)(1 - \mathcal{R}_0)\\
&= a_1\Delta \ + \ d_2\frac{X + Z}{Y}(1 - \mathcal{R}_0).
\end{aligned}$$

It remains to show that $\Delta > 0$. Using the expressions of d_2 and A,

$$\Delta = XY + YZ - p\delta\gamma + \frac{\delta\gamma(\epsilon + p\mu)}{Y}.$$

Multiplying by $Y > 0$,

$$Y\Delta = Y^2(X + Z) - p\delta\gamma Y + \delta\gamma(\epsilon + p\mu).$$

Write $Y = \mu + u$ with $u = \delta + \sigma + \eta/2 > 0$. Expanding and simplifying yields

$$\begin{aligned} Y\Delta &= (X + Z)\mu^2 + 2\mu u(X + Z) + (X + Z)u^2 - p\delta\gamma u + \delta\gamma\epsilon \\ &\geq (X + Z)\mu^2 + 2\mu u(X + Z) + (X + Z)u^2 - p\delta\gamma u^2 + \delta\gamma\epsilon \\ &\geq (X + Z)(\mu^2 + 2\mu u) + (X + Z - p\delta\gamma)u^2 + \delta\gamma\epsilon \\ &\geq (X + Z)(\mu^2 + 2\mu u) + (Z + \mu + \eta + (1 - p\delta)\gamma)u^2 + \delta\gamma\epsilon > 0. \end{aligned}$$

Hence $\Delta > 0$.
Therefore, for $\mathcal{R}_0 < 1$, we get $a_1a_2 - a_3 > 0$. All Routh–Hurwitz conditions are satisfied, so the roots of $Q(\Lambda)$ have negative real parts. Consequently $\mathcal{E}_1$ is locally asymptotically stable when $\mathcal{R}_0 < 1$.
If $\mathcal{R}_0 > 1$, then $a_3 < 0$ and the constant term of $Q(\Lambda)$ is negative, which forces at least one positive real root, hence $\mathcal{E}_1$ is unstable. □

3.4.2. Global stability analysis of the endemic equilibrium

In this section, we examine the global stability of the endemic equilibrium (EE) over the region $\mathcal{G}$, defined by

$$\mathcal{G} = \left\{(S, V, E, I, T, R) \in \mathbb{R}^6_+ : S > 0, V > 0, E > 0, I > 0, T > 0, R > 0\right\}. \tag{3.5}$$

Theorem 3.3. *The endemic equilibrium point $\mathcal{E}_2 = (S^*_2, V^*_2, E^*_2, I^*_2, T^*_2, R^*_2)$ of system* (2.1) *is globally asymptotically stable in $\mathcal{G}$ if $\mathcal{R}_0 > 1$.*

Proof. The condition $\mathcal{R}_0 > 1$ guarantees the existence of a unique endemic equilibrium point $\mathcal{E}_2$ with strictly positive components.

Consider the Lyapunov function

$$\begin{aligned} \mathcal{W}(V, S, E, I, T, R) = &\left(S - S^*_2 - S^*_2 \ln \frac{S}{S^*_2}\right) + \left(V - V^*_2 - V^*_2 \ln \frac{V}{V^*_2}\right) + \left(E - E^*_2 - E^*_2 \ln \frac{E}{E^*_2}\right) \\ &+ \left(I - I^*_2 - I^*_2 \ln \frac{I}{I^*_2}\right) + \left(T - T^*_2 - T^*_2 \ln \frac{T}{T^*_2}\right) + \left(R - R^*_2 - R^*_2 \ln \frac{R}{R^*_2}\right). \end{aligned}$$

The time derivative of $\mathcal{W}$ along the trajectories of system (2.1) is given by

$$\begin{aligned} \frac{d\mathcal{W}(V, S, E, I, T, R)}{dt} = &\left(1 - \frac{S^*_2}{S}\right)\frac{dS}{dt} + \left(1 - \frac{V^*_2}{V}\right)\frac{dV}{dt} + \left(1 - \frac{E^*_2}{E}\right)\frac{dE}{dt} \\ &+ \left(1 - \frac{I^*_2}{I}\right)\frac{dI}{dt} + \left(1 - \frac{T^*_2}{T}\right)\frac{dT}{dt} + \left(1 - \frac{R^*_2}{R}\right)\frac{dR}{dt}. \end{aligned}$$

From the endemic equilibrium point relations, we have

$$\begin{aligned} (1 - \rho)\lambda &= -kV^*_2 - \phi R^*_2 + \beta S^*_2 I^*_2 + \mu S^*_2, \\ \rho\lambda &= (k + \mu)V^*_2 + \xi V^*_2 I^*_2, \end{aligned}$$

$$
\begin{aligned}
(\epsilon+\mu)E_2^* &= \xi V_2^* I_2^* + \beta S_2^* I_2^* + \theta\beta R_2^* I_2^* + (1-p)\delta T_2^*,\\
(\mu+\eta+\gamma)I_2^* &= \epsilon E_2^* + p\delta T_2^*,\\
(\delta+\sigma+\mu+\tfrac{\eta}{2})T_2^* &= \gamma I_2^*,\\
(\mu+\phi)R_2^* &= \sigma T_2^* + \theta\beta R_2^* I_2^*.
\end{aligned}
$$

We now evaluate each component of $\frac{d\mathcal{W}}{dt}$ individually.

- For the S-compartment,

$$
\begin{aligned}
\left(1-\frac{S_2^*}{S}\right)\frac{dS}{dt} &= -\mu\frac{(S-S_2^*)^2}{S} + \beta S_2^* I_2^*\left(1-\frac{S_2^*}{S}+\frac{I}{I_2^*}-\frac{SI}{S_2^* I_2^*}\right)\\
&\quad + kV_2^*\left(\frac{V}{V_2^*}-\frac{S_2^* V}{S V_2^*}-1+\frac{S_2^*}{S}\right) + \phi R_2^*\left(\frac{R}{R_2^*}-\frac{S_2^* R}{S R_2^*}-1+\frac{S_2^*}{S}\right).
\end{aligned}
\tag{3.6}
$$

- For the V-compartment,

$$
\left(1-\frac{V_2^*}{V}\right)\frac{dV}{dt} = -(k+\mu)\frac{(V-V_2^*)^2}{V} + \xi V_2^* I_2^*\left(1-\frac{V_2^*}{V}+\frac{I}{I_2^*}-\frac{VI}{V_2^* I_2^*}\right).
\tag{3.7}
$$

- For the E-compartment,

$$
\begin{aligned}
\left(1-\frac{E_2^*}{E}\right)\frac{dE}{dt} &= -(\epsilon+\mu)\frac{(E-E_2^*)^2}{E} + \xi V_2^* I_2^*\left(\frac{VI}{V_2^* I_2^*}-\frac{E_2^* VI}{E V_2^* I_2^*}+\frac{E_2^*}{E}-1\right)\\
&\quad + \beta S_2^* I_2^*\left(\frac{SI}{S_2^* I_2^*}-\frac{E_2^* SI}{E S_2^* I_2^*}+\frac{E_2^*}{E}-1\right) + \theta\beta R_2^* I_2^*\left(\frac{RI}{R_2^* I_2^*}-\frac{E_2^* RI}{E R_2^* I_2^*}+\frac{E_2^*}{E}-1\right)\\
&\quad + (1-p)\delta T_2^*\left(\frac{T}{T_2^*}-\frac{E_2^* T}{E T_2^*}+\frac{E_2^*}{E}-1\right).
\end{aligned}
\tag{3.8}
$$

- For the I-compartment,

$$
\begin{aligned}
\left(1-\frac{I_2^*}{I}\right)\frac{dI}{dt} &= -(\mu+\eta+\gamma)\frac{(I-I_2^*)^2}{I} + \epsilon E_2^*\left(\frac{E}{E_2^*}-\frac{I_2^* E}{I E_2^*}+\frac{I_2^*}{I}-1\right)\\
&\quad + p\delta T_2^*\left(\frac{T}{T_2^*}-\frac{I_2^* T}{I T_2^*}+\frac{I_2^*}{I}-1\right).
\end{aligned}
\tag{3.9}
$$

- For the T-compartment,

$$
\left(1-\frac{T_2^*}{T}\right)\frac{dT}{dt} = -\left(\delta+\sigma+\mu+\frac{\eta}{2}\right)\frac{(T-T_2^*)^2}{T} + \gamma I_2^*\left(\frac{I}{I_2^*}-\frac{IT_2^*}{I_2^* T}+\frac{T_2^*}{T}-1\right).
\tag{3.10}
$$

- For the R-compartment,

$$
\begin{aligned}
\left(1-\frac{R_2^*}{R}\right)\frac{dR}{dt} &= -(\mu+\phi)\frac{(R-R_2^*)^2}{R} + \sigma T_2^*\left(-1+\frac{R_2^*}{R}+\frac{T}{T_2^*}-\frac{TR_2^*}{T_2^* R}\right)\\
&\quad + \theta\beta R_2^* I_2^*\left(1-\frac{R_2^*}{R}+\frac{I}{I_2^*}-\frac{RI}{R_2^* I_2^*}\right).
\end{aligned}
\tag{3.11}
$$

Combining expressions (3.6)–(3.11), we obtain

$$\begin{aligned}\frac{d\mathcal{W}}{dt} =& -\mu\frac{(S-S_2^*)^2}{S} - (k+\mu)\frac{(V-V_2^*)^2}{V} - (\epsilon+\mu)\frac{(E-E_2^*)^2}{E}\\ &- (\mu+\eta+\gamma)\frac{(I-I_2^*)^2}{I} - \left(\delta+\sigma+\mu+\frac{\eta}{2}\right)\frac{(T-T_2^*)^2}{T} - (\mu+\phi)\frac{(R-R_2^*)^2}{R}\\ &+ \beta S_2^* I_2^*\left(3 - \frac{S_2^*}{S} - \frac{E_2^* S I}{E S_2^* I_2^*} - \frac{I_2^* E}{I E_2^*}\right) + \xi V_2^* I_2^*\left(3 - \frac{V_2^*}{V} - \frac{E_2^* V I}{E V_2^* I_2^*} - \frac{I_2^* E}{I E_2^*}\right)\\ &+ \theta\beta R_2^* I_2^*\left(3 - \frac{R_2^*}{R} - \frac{E_2^* R I}{E R_2^* I_2^*} - \frac{I_2^* E}{I E_2^*}\right) + (1-p)\delta T_2^*\left(3 - \frac{T_2^* I}{T I_2^*} - \frac{E_2^* T}{E T_2^*} - \frac{I_2^* E}{I E_2^*}\right)\\ &+ k V_2^*\left(2 - \frac{V_2^* S}{S_2^* V} - \frac{S_2^* V}{S V_2^*}\right) + \phi R_2^*\left(2 - \frac{R_2^* S}{R S_2^*} - \frac{S_2^* R}{S R_2^*}\right)\\ &+ p\delta T_2^*\left(2 - \frac{I_2^* T}{I T_2^*} - \frac{T_2^* I}{T I_2^*}\right) + \sigma T_2^*\left(2 - \frac{T_2^* R}{T R_2^*} - \frac{R_2^* T}{R T_2^*}\right).\end{aligned} \tag{3.12}$$

Using the equilibrium system, we obtain that the product of the three dimensionless terms in each interaction bracket equals one, which allows the application of the arithmetic–geometric mean inequality. Hence, each bracketed term satisfied:

$$\begin{cases} 3 - \frac{S_2^*}{S} - \frac{E_2^* S I}{E S_2^* I_2^*} - \frac{I_2^* E}{I E_2^*} \le 0,\\ 3 - \frac{V_2^*}{V} - \frac{E_2^* V I}{E V_2^* I_2^*} - \frac{I_2^* E}{I E_2^*} \le 0,\\ 3 - \frac{R_2^*}{R} - \frac{E_2^* R I}{E R_2^* I_2^*} - \frac{I_2^* E}{I E_2^*} \le 0,\\ 3 - \frac{T_2^* I}{T I_2^*} - \frac{E_2^* T}{E T_2^*} - \frac{I_2^* E}{I E_2^*} \le 0,\\ 2 - \frac{V_2^* S}{S_2^* V} - \frac{S_2^* V}{S V_2^*} \le 0,\\ 2 - \frac{R_2^* S}{R S_2^*} - \frac{S_2^* R}{S R_2^*} \le 0,\\ 2 - \frac{I_2^* T}{I T_2^*} - \frac{T_2^* I}{T I_2^*} \le 0,\\ 2 - \frac{T_2^* R}{T R_2^*} - \frac{R_2^* T}{R T_2^*} \le 0. \end{cases} \tag{3.13}$$

Moreover, from the structure of (3.12), all the non-positive terms vanish simultaneously if and only if

$$(S, V, E, I, T, R) = (S_2^*, V_2^*, E_2^*, I_2^*, T_2^*, R_2^*).$$

Therefore, the set

$$\left\{(S, V, E, I, T, R) \in \mathcal{G} : \frac{d\mathcal{W}}{dt} = 0\right\}$$

reduces to the singleton $\mathcal{E}_2$. Since each term in the time derivative of the Lyapunov function is non-positive, it follows that

$$\frac{d\mathcal{W}}{dt} \le 0 \quad \text{for all } \mathcal{R}_0 > 1.$$

Consequently, by LaSalle's Invariance Principle [38], the endemic equilibrium point $\mathcal{E}_2$ is globally asymptotically stable in $\mathcal{G}$. □

4. Estimation of parameters and numerical simulation

This section focuses on estimating model parameters to align theoretical predictions with observed epidemiological data. Eight key parameters are calibrated using tuberculosis incidence data from the Global Tuberculosis Report [39] spanning 1990 to 2024. The remaining parameters are adopted from established literature to ensure biological and epidemiological plausibility.

4.1. Estimation of parameters

Parameter estimation for the model is conducted using demographic and public health data specific to Algeria during the 1990–2024 period. Each parameter is derived from reliable sources, and its calculation is detailed below.

- **Recruitment rate (λ)**: Representing the average annual number of births, this rate is estimated from Algerian demographic statistics [40] as $\lambda = 926{,}955$ individuals per year.
- **Natural mortality rate (μ)**: The natural mortality rate μ is defined as the per-capita crude death rate, i.e., the observed annual number of natural deaths divided by the total population. This value is obtained from the average crude death rate in Algeria over the study period (1990–2024) [40]. Using the crude death rate rather than the reciprocal of life expectancy is appropriate for compartmental models that do not explicitly account for age structure, particularly in populations with a relatively young age distribution such as Algeria's. While the reciprocal of life expectancy (approximately $(0.013 - -0.014)\,\text{year}^{-1}$ for 72–77 years) assumes a stationary and homogeneous age distribution, it tends to overestimate the effective natural mortality rate in such settings. Based on demographic data, the average crude death rate over the 35-year period is $\mu = 0.004985714\,\text{year}^{-1}$, which is rounded to $\mu \approx 0.005\,\text{year}^{-1}$ and used in the model.
- **Vaccination rate (ρ)**: Defined as the proportion of infants aged 12–23 months receiving the BCG vaccine. Based on World Bank data from official sources [33], the average coverage is $\rho = 0.977$.
- **Vaccine waning rate (k)**: This parameter represents the rate at which vaccine-induced immunity declines, returning individuals to the susceptible class. International systematic reviews by [41, 42] suggest a typical protection window of 10–15 years, while some cohort studies report effectiveness persisting for 20 years or more [43]. In the Algerian context, where BCG vaccination is mandatory at birth with coverage consistently exceeding 99%, we assume a mean protection duration of approximately 16 years. This value represents a conservative estimate within the range of published evidence, reflecting the robustness of the national neonatal immunization program while accounting for the observed epidemiological shift wherein susceptibility increases as individuals transition into late adolescence and early adulthood. The corresponding waning rate is therefore $k = 1/16 = 0.0625\,\text{year}^{-1}$.
- **Fraction of treatment failure (p)**: Based on Algerian TB treatment data (2000–2021) [33], a treatment success rate of 89.05% corresponds to a failure fraction of $p = 0.1095$, representing the proportion of patients who do not successfully complete treatment.

These parameters form the demographic and intervention foundation of the model, enabling a realistic simulation of tuberculosis transmission dynamics in Algeria.

The main requirements were carefully selected and are listed below: According to [40], the total starting population, $N(0)$, was determined to be 25,518,074, which corresponds to the population of

Algeria in 1990. The World Health Organization TB Report [39] provided the first infected group, $I(0)$, or 11,607. 8852 was assumed to represent the first exposed group, $E(0)$. Furthermore, the recovered people were set to 10,000, and the initial treated group, $T(0)$, was specified as 20,000. 8,109,389 was determined to be the count of vaccinated people, $V(0)$. The initial susceptibility group was therefore determined to be $S(0) = N(0) - E(0) - I(0) - T(0) - V(0) - R(0) = 17{,}358{,}226$. The goal of these carefully chosen beginning conditions was to guarantee accurate and reliable numerical simulations for the system under study.

The remaining model parameters were estimated by fitting the numerical solution of the SVEITRS system (2.1) to the observed tuberculosis (TB) case data. The parameter estimation process was performed using MATLAB's `fmincon` solver, which is a gradient-based nonlinear optimization tool capable of handling constrained problems. The fitting procedure aimed to minimize the discrepancy between the observed and model-predicted TB cases, quantified by the mean squared error (MSE):

$$\text{MSE} = \frac{1}{n}\sum_{i=1}^{n}\left(Y_i^{\text{obs}} - Y_i^{\text{pred}}\right)^2, \tag{4.1}$$

where n denotes the total number of observations, Y_i^{obs} represents the reported TB cases, and Y_i^{pred} represents the corresponding model predictions. To ensure that the estimated parameters remain within biologically and epidemiologically plausible ranges, strict lower and upper bounds were applied during optimization. This constrained approach reduces the risk of convergence to local optima, thereby enhancing the reliability, uniqueness, and interpretability of the fitted parameters. The methodology reflects a widely accepted practice in epidemiological modeling, combining data-driven calibration with mechanistic insights to support robust predictions and evidence-based decision-making.

Figure 2 presents the simulation results for system (2.1) using the optimized parameters from Table 2, providing a detailed comparison between observed TB case data and the model's predictions from 1990 to 2024. The simulation demonstrates an optimal fit to the empirical data, highlighting the superior descriptive capability of the model and its increased effectiveness in capturing the dynamics of TB transmission in Algeria.

Table 2. Model parameters and initial conditions used to simulate tuberculosis dynamics in Algeria.

Parameters	Value	Units	Source
$S(0)$	17,358,226	Individual	Calculated
$V(0)$	8,109,388	Individual	Assumed
$E(0)$	8852	Individual	Assumed
$I(0)$	11,607	Individual	[39]
$T(0)$	20,000	Individual	Assumed
$R(0)$	10,000	Individual	Assumed
λ	926,955	Individual $\cdot$ Year^{-1}	[40]
β	5×10^{-11}	Individual $\cdot$ Year^{-1}	Fitted
k	0.0625	Year^{-1}	Assumed
δ	0.0158	Year^{-1}	Fitted
θ	0.01	Dimensionless	Fitted
γ	0.7145	Year^{-1}	Fitted
ξ	3×10^{-13}	Individual^{-1} $\cdot$ Year^{-1}	Fitted
μ	0.005	Year^{-1}	[40]
p	0.1095	Dimensionless	[33]
ϵ	0.0818	Year^{-1}	Fitted
η	0.01	Year^{-1}	Fitted
ρ	0.977	Dimensionless	[44]
ϕ	5×10^{-5}	Year^{-1}	Fitted
σ	0.0223	Year^{-1}	Fitted

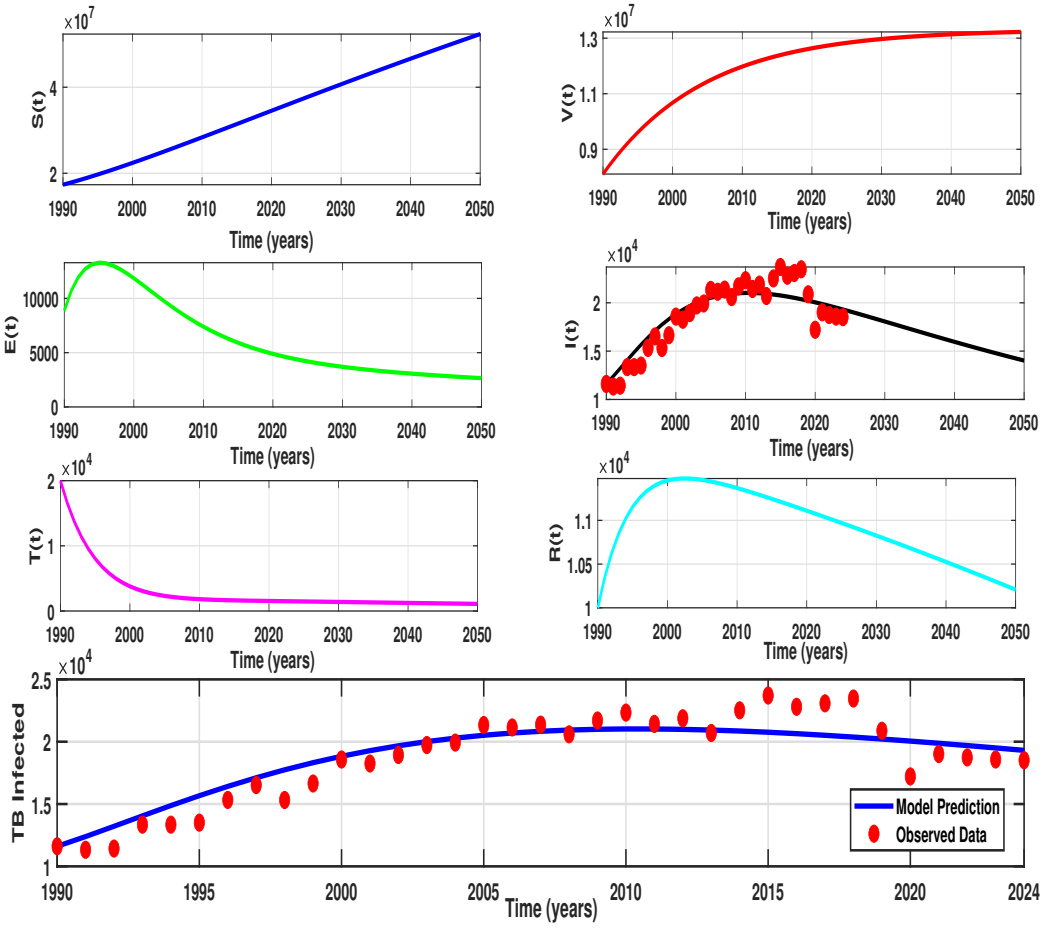

Figure 2. Evolution in time of system (2.1) with the optimal parameters given in Table 2. A comparison of the reported TB incidence statistics from 1990 to 2024 with the simulated infected populations for the model, as well as the projected evolution of the TB pandemic from 1990 to 2050.

4.2. Sensitivity analysis

The partial rank correlation coefficient (PRCC) method is employed to perform a sensitivity analysis of the parameters in the proposed tuberculosis (TB) model. This approach assesses how sensitive key model outputs, particularly the infected population and the basic reproduction number ($\mathcal{R}_0$), are to individual input parameters, while accounting for the interactions among other parameters. To conduct the analysis, Latin hypercube sampling (LHS) is used to generate a broad spectrum of parameter combinations. The model is subsequently simulated using these sampled parameter sets, and PRCC values are computed to quantify the influence of each parameter on the model outcomes. This procedure provides a systematic evaluation of how each parameter impacts the disease dynamics. LHS ensures that the parameter space is sampled representatively by creating 1000 parameter sets from the given minimum and maximum ranges. While taking into consideration the effect of other factors, the PRCC approach ranks each parameter's influence according to how strongly it corresponds with the output variable.

The PRCC-based sensitivity analysis (Figure 3) highlights a clear ranking in the relative impact of model parameters on the infectious population. The population recruitment rate λ (PRCC ≈ 0.944) and the transmission coefficient β (PRCC ≈ 0.932) emerge as the most influential parameters, both exerting a strong positive effect on disease prevalence. In contrast, the natural mortality rate μ demonstrates the strongest negative association (PRCC ≈ -0.83), thereby acting as the main mitigating factor.

With respect to control-related parameters, the treatment rate γ shows a moderate inverse correlation with infection levels (PRCC ≈ -0.371), indicating that therapeutic interventions contribute meaningfully to reducing disease burden, albeit less prominently than transmission-related mechanisms.

Vaccination-associated parameters, however, exhibit negligible sensitivity. Both vaccine coverage ρ (PRCC ≈ -0.015) and the immunity waning rate k (PRCC ≈ 0.015) present values close to zero, reflecting a limited direct influence on the infectious class. Likewise, parameters including the recovery rate σ (PRCC ≈ -0.103), vaccine failure rate ξ (PRCC ≈ 0.078), and disease progression rate ϵ (PRCC ≈ 0.079) display relatively low sensitivity magnitudes ($|\text{PRCC}| \lesssim 0.1$), suggesting that their individual effects are secondary when compared with demographic and transmission drivers.

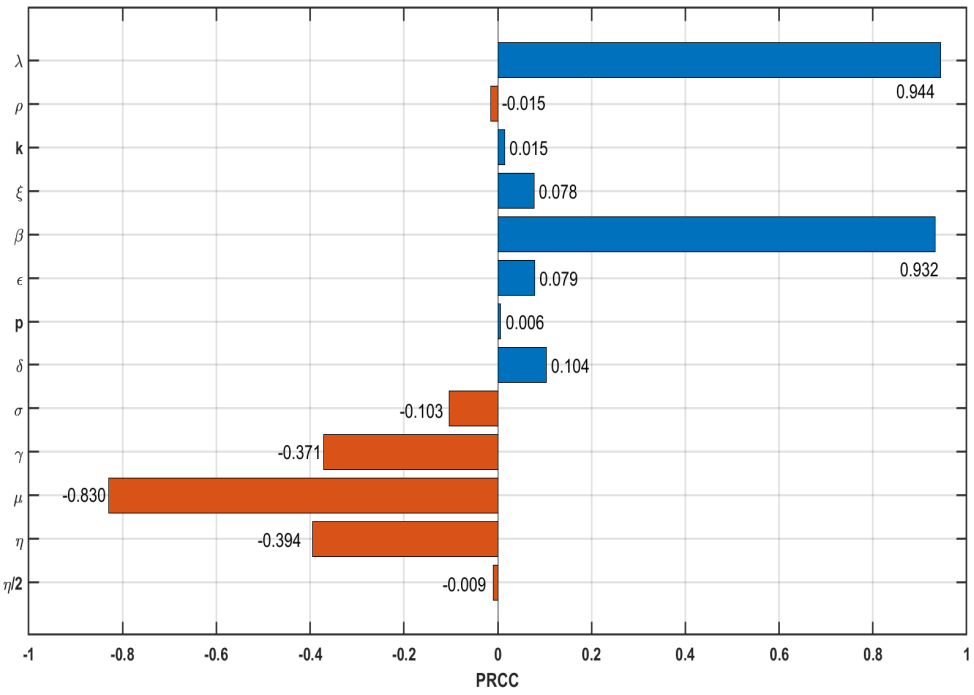

Figure 3. The partial rank correlation coefficient (PRCC) results showing the sensitivity of the infected population to model parameters.

To further investigate the combined impact of key model parameters and to address the non-linear interactions within TB dynamics, a bivariate sensitivity analysis was conducted using 3D surface plots presented in Figure 4. These visualizations provide a comprehensive view of how the basic reproduction number ($\mathcal{R}_0$) responds to the simultaneous variation of two parameters. As shown in Figures 4(a) and (b), the interaction of the transmission rate (β) with vaccine coverage (ρ) and the

treatment rate (γ) illustrates that, while β is a primary driver of the surface's elevation, both ρ and γ exert a consistent downward pressure on $\mathcal{R}_0$. The transition from yellow to blue regions on the surfaces indicates that increasing vaccination and treatment efforts effectively lowers the "floor" of the epidemic potential, even under relatively high transmission conditions.

Furthermore, the 3D analysis of the waning immunity rate (k) and the reactivation rate (δ) in relation to β (Figures 4(c), and (d)) reveals their roles as multipliers of infectious pressure. The $\mathcal{R}_0$ surface becomes significantly steeper and reaches higher peaks as these biological parameters increase, confirming that the loss of vaccine-induced protection and the reactivation of latent cases substantially exacerbate the impact of primary transmission.

These interaction surfaces complement the individual parameter rankings obtained from the PRCC, providing a more holistic understanding of how integrated control strategies combining preventive measures, sustained vaccination, and effective treatment can synergistically stabilize disease dynamics and maintain $\mathcal{R}_0$ below the critical threshold of unity.

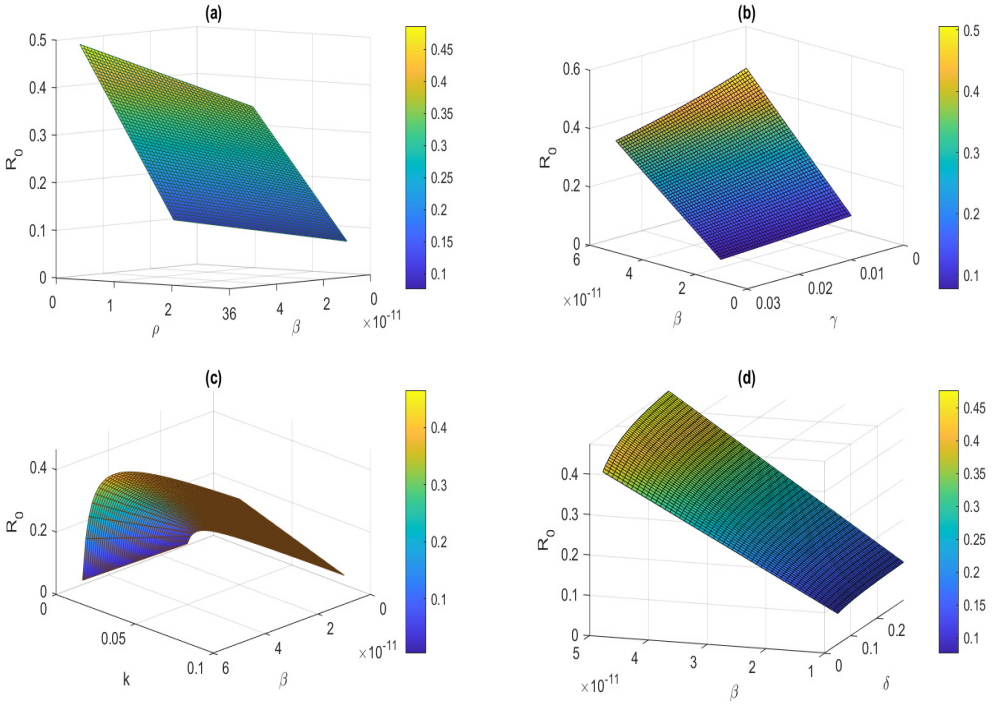

Figure 4. Influence of system parameters on the threshold reproduction number $\mathcal{R}_0$.

5. Numerical results and discussion

The estimated parameters of the tuberculosis model are presented in Table 2. Figure 2 displays the reported tuberculosis incidence data alongside the fitted trajectory obtained using the optimized parameter values. The model successfully captures the overall temporal evolution of tuberculosis incidence in Algeria, and the long-term forecast (2024–2050) depicted provides a detailed epidemiological insight into the disease dynamics. Specifically, the model predicts a consistent decline

in both exposed $E(t)$ and infectious $I(t)$ populations. This downward trend is a direct consequence of the sustained efficacy of isolation and treatment protocols. Notably, the treatment class $T(t)$ approaches zero toward 2050, which signifies that the disease burden is being reduced to a point where fewer individuals require clinical intervention. Furthermore, the stabilization of the vaccinated class $V(t)$ at a high threshold acts as a biological barrier, preventing secondary outbreaks despite the natural increase in the susceptible population $S(t)$. These combined dynamics provide a theoretical guarantee that the basic reproduction number $\mathcal{R}_0$ remains below unity in the long run, leading to the eventual eradication of the disease.

The goodness-of-fit assessment indicates a coefficient of determination of $R^2 = 0.84$, which reflects a satisfactory agreement between the model predictions and the observed data. This result suggests that the integer-order formulation, based on classical first-order derivatives, is able to describe a substantial portion of the variability in tuberculosis transmission dynamics.

Furthermore, using the parameter values reported in Table 2, we obtain the analytical coefficients $a_1 \approx 0.30$, $a_2 \approx 0.023$, and $a_3 \approx 0.00016$. It follows that

$$a_1 a_2 \approx 0.0069 > a_3 \approx 0.00016.$$

Moreover, with $\mathcal{R}_0 \approx 0.44 < 1$, all Routh–Hurwitz conditions for the cubic polynomial associated with the Jacobian matrix at the disease-free equilibrium (DFE) are satisfied. Therefore, the DFE is locally asymptotically stable.

Table 3 summarizes the main epidemiological indicators derived from the fitted model parameters alongside typical values reported in the literature.

Table 3. Key epidemiological indicators of tuberculosis (TB) in Algeria: Comparison between model estimates and typical reported values.

Indicator	**Model estimate**	**Typical value (Algeria)**	**Epidemiological interpretation**
Basic reproduction number ($\mathcal{R}_0$)	0.44	< 1 (low transmission setting)	Reflects the impact of BCG vaccination, early diagnosis, and treatment programs in Algeria, which maintain TB transmission below the epidemic threshold.
Average latent period	≈ 11.52 years	5–10 years (can extend to decades)	Long latency reflects delayed progression; consistent with partial immunity due to BCG and slow reactivation dynamics.
Average infectious period	≈ 1.37 years	6–12 months (untreated cases may last longer)	Slightly higher than typical values; may reflect diagnostic delays or incomplete/late treatment in some cases.

Table 3 shows strong agreement between the model estimates and TB epidemiology in Algeria. The low basic reproduction number ($\mathcal{R}_0 = 0.44$) indicates controlled transmission, attributed to the

effectiveness of the BCG vaccination and the directly observed treatment (DOTS) programs [32]. The prolonged latent period ($\frac{1}{\mu+\epsilon} \approx 11.52$ years) reflects a chronic "silent reservoir" of latent infections, while the infectious period ($\frac{1}{\gamma+\mu+\eta} \approx 1.37$ years) accounts for diagnostic delays and undetected cases. These findings highlight the importance of continued surveillance and the need for earlier case detection to further reduce the community infectious pool [45].

To provide quantitative guidance for TB control in Algeria, we simulated three distinct intervention scenarios starting from 2024 (Figure 5). Under the no-intervention scenario (business-as-usual), the infected population $I(t)$ continues a slow natural decline but remains at high levels. A moderate intervention, characterized by a 10% reduction in the transmission rate (β) and a 20% increase in the treatment rate (γ), accelerates this decline significantly. Furthermore, we simulated an aggressive intervention scenario. This scenario represents a high-protection combined strategy, where the vaccine failure rate (ξ) is substantially reduced, reflecting a vaccine with 90% efficacy, and the treatment rate (γ) is increased by 70%. As illustrated in Figure 5, while this integrated approach yields the most superior epidemiological outcome, reducing active cases significantly by 2035, the infected population does not reach zero within the forecast period. This quantitative evidence supports our conclusion that while vaccination and treatment are pivotal, they are insufficient alone to achieve total TB eradication in the near term without additional interventions targeting latent reservoirs and transmission chains.

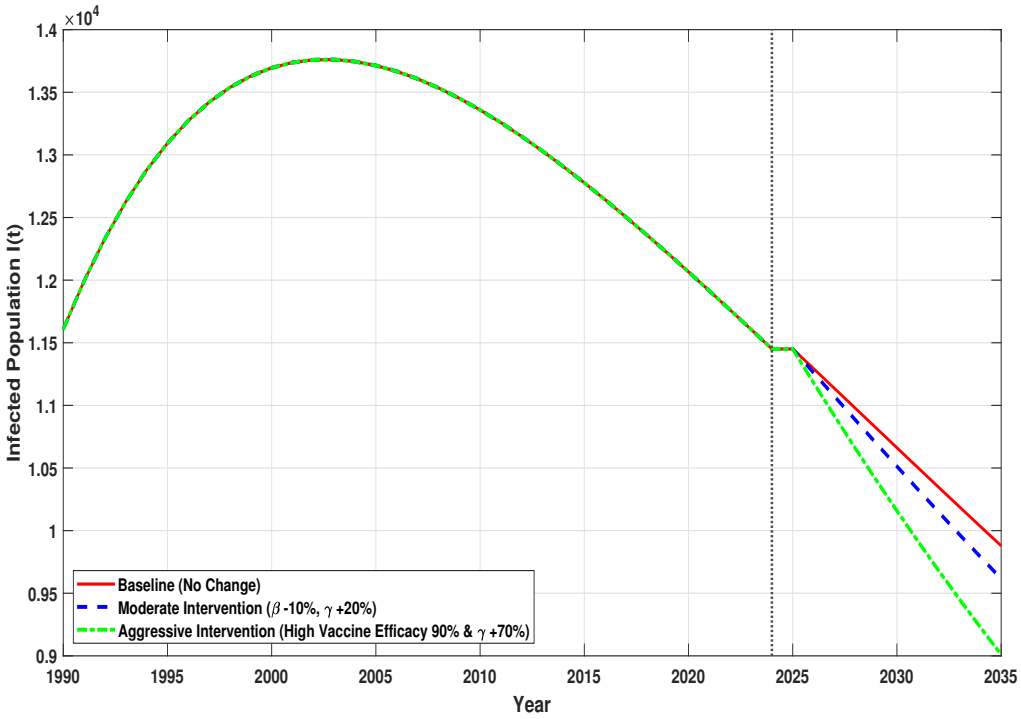

Figure 5. Projected impact of three intervention strategies (no intervention, moderate intervention, and aggressive intervention) starting from 2024 to 2035 on the infected population $I(t)$.

As illustrated in Figure 6, the infection dynamics are sensitive to key epidemiological parameters. The progression rate ϵ (Figure 6(b)) exhibits the strongest influence: Modest increases sharply raise

the infection peak and accelerate the epidemic onset. The transmission rate β (Figure 6(a)) and the endogenous reactivation rate δ (Figure 6(c)) also substantially elevate endemic levels. In contrast, the exogenous reinfection rate θ (Figure 6(d)) produces a comparatively weaker effect within the examined range, likely because recovered individuals constitute a smaller pool and retain partial immunity.

Biologically, higher β facilitates transmission; increased ϵ rapidly activates the large latent reservoir; and elevated δ or θ reintroduces individuals into the infectious pool, sustaining transmission. These results suggest that interventions targeting latent progression (e.g., preventive therapy) and transmission reduction may yield the most immediate impact on TB prevalence.

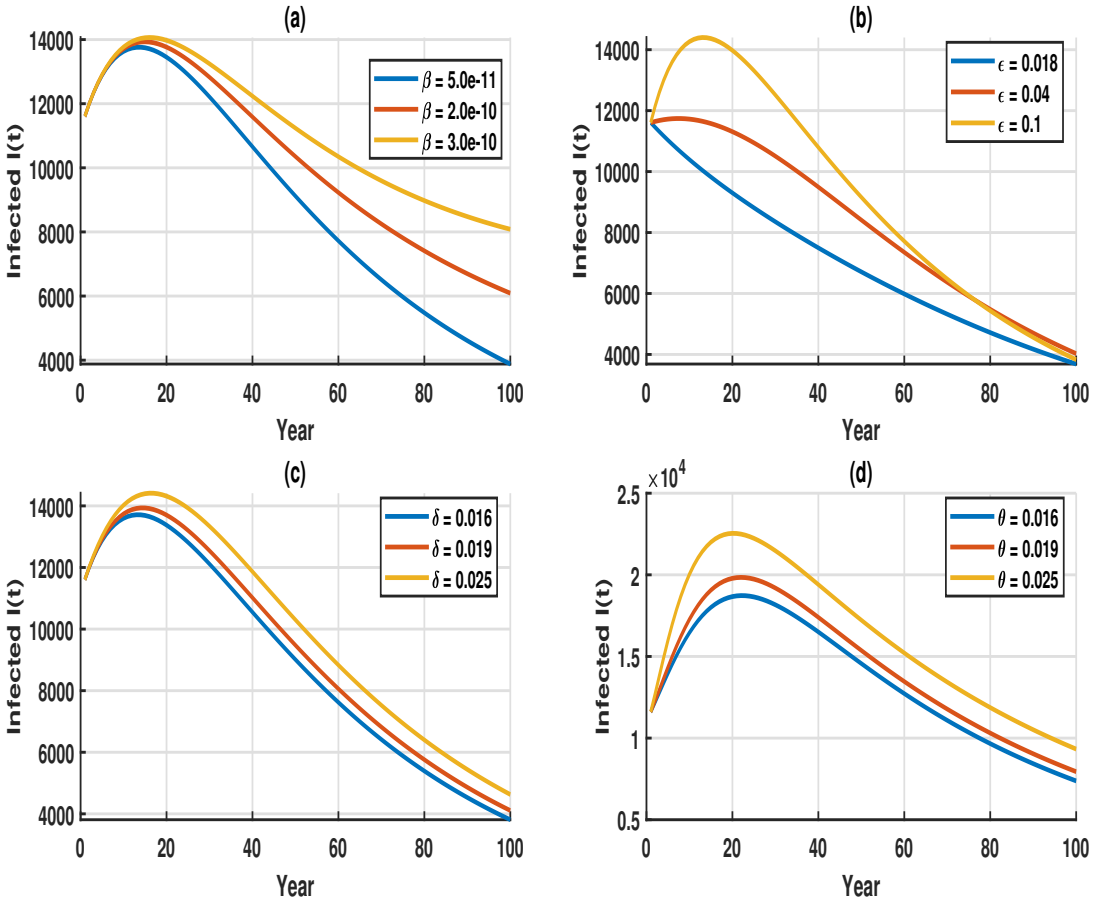

Figure 6. The effect of transmission rate β, normal development rate ϵ, endogenous reactivation rate δ, and exogenous reinfection rate θ on the infected class $I(t)$. Panels (a)–(d) show that increasing these parameters elevates the infection peak and endemic levels. The dynamics exhibit high sensitivity to ϵ, which significantly accelerates the epidemic onset, while θ shows a relatively weaker impact.

Figure 7 illustrates the effect of the vaccine failure rate (breakthrough infection rate) ξ on the dynamics of all model compartments. As ξ increases, the populations of exposed (E), infected (I), and treated (T) individuals rise significantly. This occurs because higher ξ reduces the protective effect of the vaccine, allowing individuals in the vaccinated class (V) to become exposed (E) more easily. In this

way, the vaccinated population no longer serves as a barrier to transmission but instead contributes to new infections. This "leakage" in vaccine effectiveness amplifies the epidemic, leading to higher peaks and a sustained endemic level. These results highlight that, beyond coverage, the vaccine's quality, specifically its ability to prevent infection (ξ remaining low), is crucial for controlling the outbreak and minimizing the long-term TB burden.

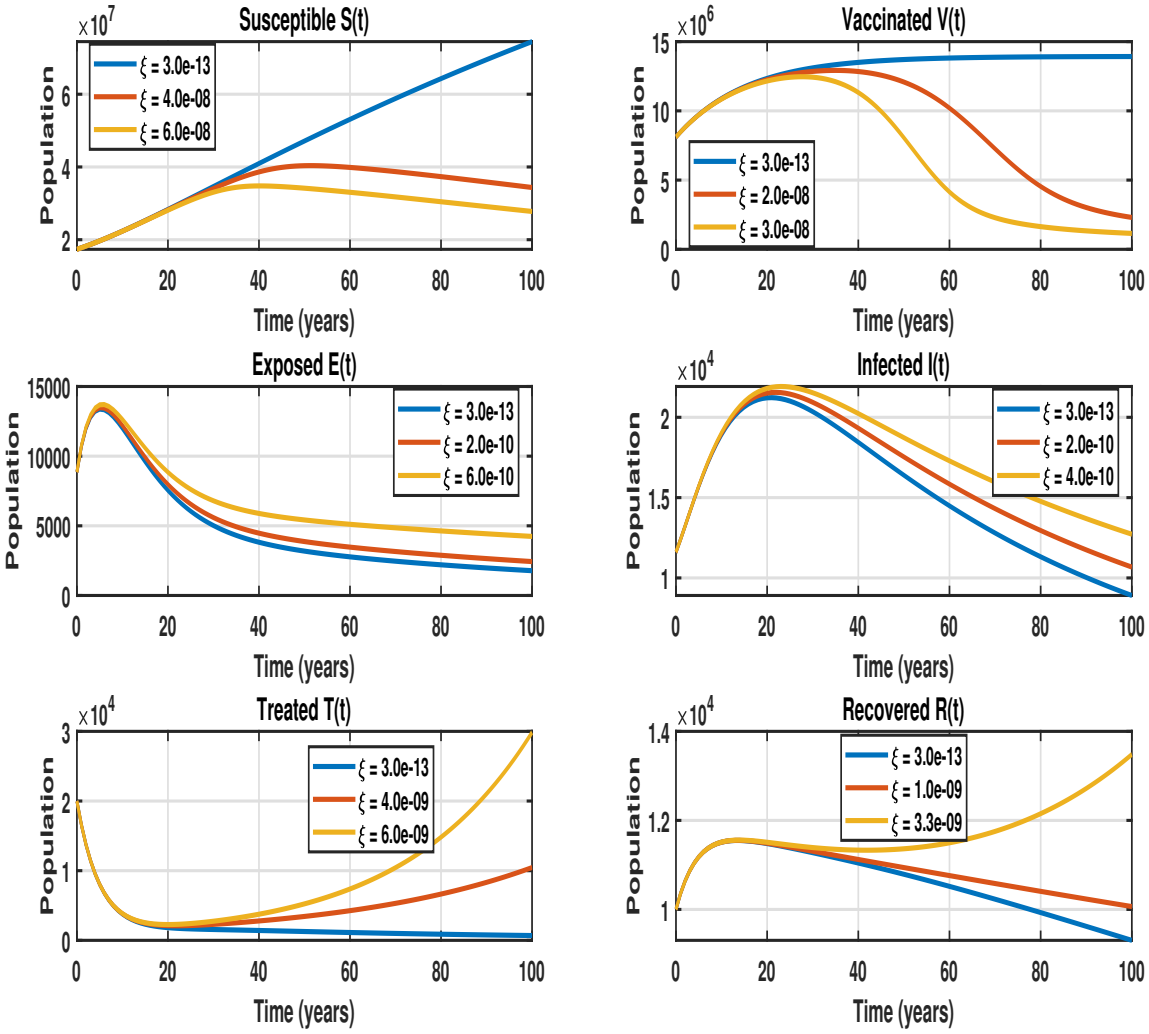

Figure 7. Effect of the vaccine failure rate ξ on the temporal dynamics of the model compartments. Increasing ξ leads to higher infection levels (E, I, T) and weakens the protective role of vaccination (V).

The temporal dynamics of the model compartments with and without immunization are shown in Figure 8. The simulation findings unequivocally show that, in comparison to the non-vaccinated scenario, the vaccination approach significantly reduces the exposed (E) and infected (I) populations by increasing the vaccinated population (V) while decreasing susceptibles (S). As a consequence, fewer

people need therapy (T) or enter the recovered class (R). This demonstrates how well the immunization program works to stop the spread of the disease and lessen the epidemic's overall impact.

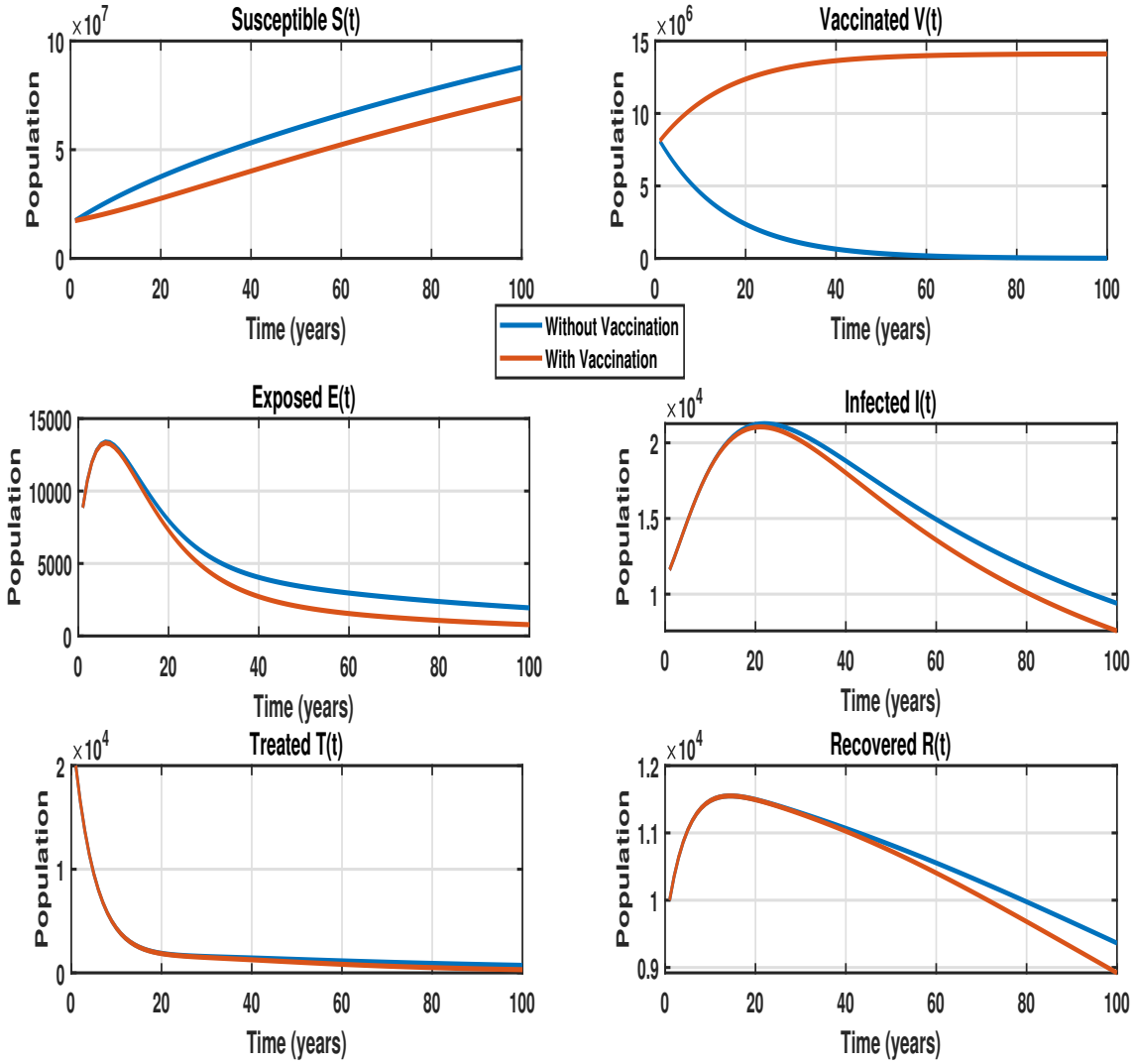

Figure 8. Comparative analysis of disease dynamics under vaccination and non-vaccination scenarios. The vaccination strategy suppresses the peaks of the exposed (E) and infected (I) populations by reducing the susceptible pool (S) and expanding the vaccinated class (V).

Figure 9 demonstrates the impact of the recovery rate σ on the system's dynamics. Increasing σ accelerates the transition from the treated (T) to the recovered (R) compartment, resulting in a substantial accumulation of recovered individuals. Consequently, the disease burden diminishes, as evidenced by the decline in the exposed (E), infectious (I), and treated (T) populations.

Although recovered individuals may gradually return to the susceptible compartment (S) via waning immunity at rate ϕ, this flow is negligible compared to the rapid recovery, and the vaccinated

compartment (V) remains unaffected. This behavior highlights that shortening the effective treatment period not only clears active cases faster but also minimizes the window for treatment failure or relapse, thereby cutting off re-entry pathways into the infectious pool and enhancing overall epidemic control.

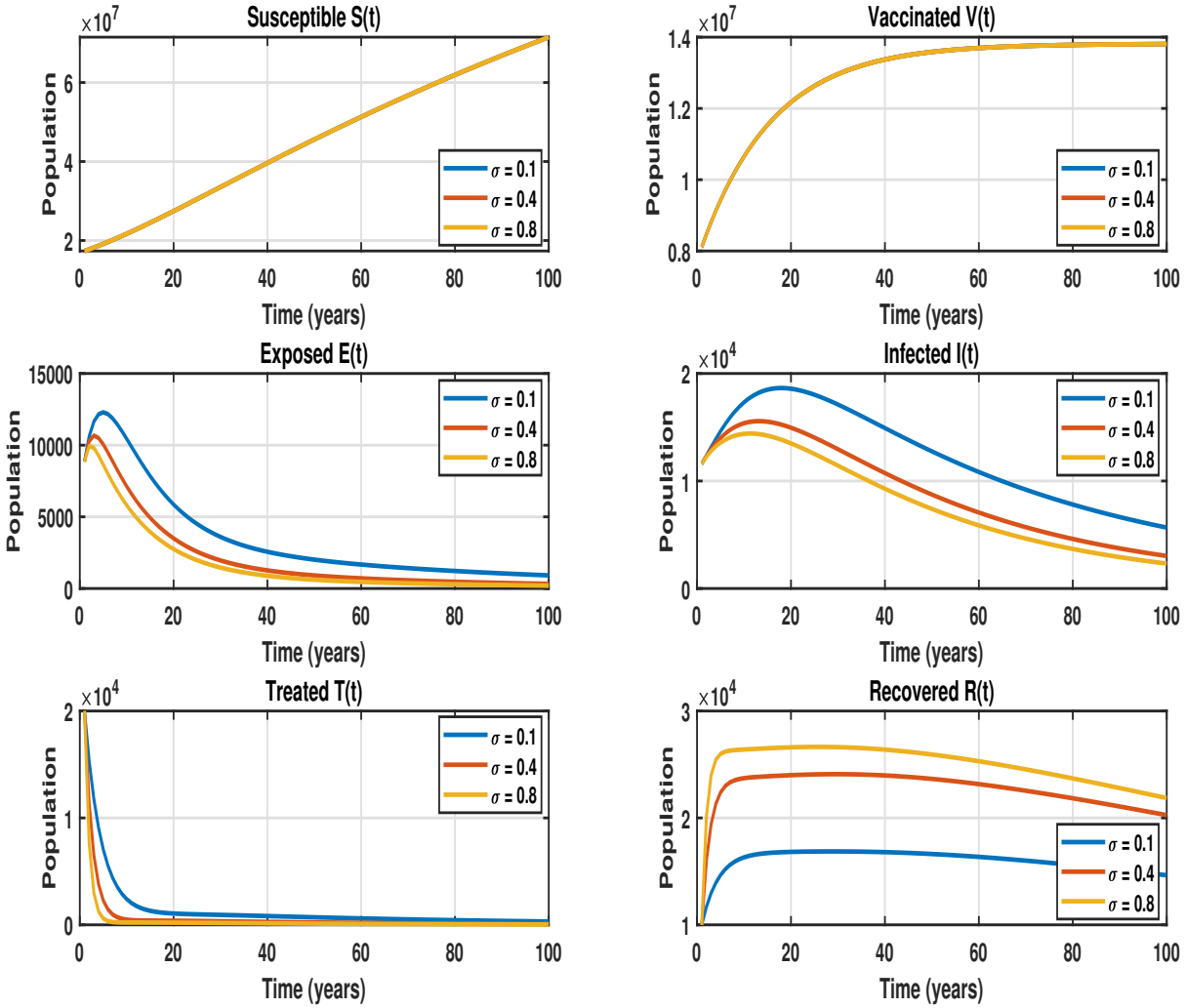

Figure 9. Impact of the recovery rate σ on TB dynamics. Increasing σ accelerates the transition from treatment (T) to recovery (R), reducing the exposed (E) and infected (I) populations and shortening the overall disease duration.

6. Conclusions

In this study, we developed and analyzed a deterministic SVEITRS compartmental model to investigate tuberculosis (TB) transmission dynamics in Algeria from 1990 to 2024. By explicitly incorporating partial vaccine efficacy, waning immunity, endogenous reactivation, and exogenous reinfection, the model provides a realistic representation of TB propagation. Theoretical analysis established stability conditions for both disease-free and endemic equilibria based on the epidemic threshold, while model calibration against epidemiological data confirmed its predictive reliability ($R^2 = 0.84$).

The sensitivity analysis, combining partial rank correlation coefficients (PRCCs) and bivariate 3D surface plots, provided a holistic understanding of the epidemic drivers. While PRCCs highlighted the dominance of transmission (β) and recruitment rates, the 3D interaction surfaces revealed the non-linear synergy between parameters. Specifically, these visualizations demonstrated that while increasing vaccination (ρ) and treatment (γ) contributes to reducing the epidemic burden, their impact remains secondary compared to transmission-related parameters. Conversely, the analysis confirmed that the waning of vaccine-induced protection (k) and the reactivation of latent cases (δ) act as significant amplifiers of infectious pressure.

Numerical simulations and long-term forecasts (2024–2050) offer optimistic yet cautious insights. The model predicts a consistent decline in both exposed and infectious populations, with the treatment class showing a marked reduction toward minimal levels by 2050, provided that current protocols are sustained. The stabilization of the vaccinated class acts as a critical biological barrier against secondary outbreaks. However, the comparison of different intervention scenarios (no intervention, moderate, and aggressive) reveals a crucial finding: Even under an aggressive strategy (characterized by 90% vaccine efficacy and a 70% increase in treatment rates), the infected population significantly declines but does not reach zero within the forecast period.

These findings indicate that, as demonstrated by the intervention scenario analysis, vaccination and treatment alone are insufficient to achieve total TB eradication in the near term. Effective control strategies must therefore go beyond clinical interventions and prioritize transmission suppression and latent reservoir management. This includes intensifying early case detection, implementing isolation strategies for active cases, and enhancing public awareness in high-risk settings. Overall, this study provides a robust quantitative framework to support evidence-based TB control strategies and highlights the necessity of integrated, multi-layered interventions for long-term disease mitigation in Algeria.

Future extensions of this work could incorporate spatial heterogeneity or fractional-order derivatives to capture memory effects and regional differences, further enhancing model realism and applicability for TB control strategies. Moreover, the model can be extended to explicitly include a subclinical (asymptomatic infectious) compartment, allowing for a more comprehensive representation of TB transmission dynamics and enabling better assessment of intervention strategies targeting silent carriers.

Author contributions

Conceptualization: Rayane Boucherma, Yakup Yildirim, Messaoud Berkal, and Mohammed-Salah Abdelouahab; Methodology: Rayane Boucherma, Mohammed-Salah Abdelouahab, and Messaoud Berkal; Software: Rayane Boucherma, Mohammed-Salah Abdelouahab, Messaoud Berkal, and Taha Radwan; Formal analysis: Rayane Boucherma, Messaoud Berkal, and Mohammed-Salah Abdelouahab; Validation: Rayane Boucherma, Messaoud Berkal, Mohammed-Salah Abdelouahab, and Taha Radwan; Investigation: Rayane Boucherma, Messaoud Berkal, Mohammed-Salah Abdelouahab, Taha Radwan, Yakup Yildirim, and Karim K. Ahmed; Resources: Taha Radwan, and Karim K. Ahmed; Writing–original draft: Rayane Boucherma, Mohammed-Salah Abdelouahab, and Messaoud Berkal; Writing–review and editing: Mohammed-Salah Abdelouahab, Yakup Yildirim, Taha Radwan, and Karim K. Ahmed; Visualization: Rayane Boucherma, Mohammed-Salah Abdelouahab, Taha Radwan, and Karim K. Ahmed; Supervision: Mohammed-Salah Abdelouahab; Funding acquisition: Taha Radwan. All authors have read and agreed to the published version of the manuscript.

Use of Generative-AI tools declaration

The authors declare that no Artificial Intelligence (AI) tools were used in the preparation of this manuscript.

Acknowledgments

The Researchers would like to thank the Deanship of Graduate Studies and Scientific Research at Qassim University for financial support (QU-APC-2026).

Conflict of interest

The authors declare that they have no conflicts of interest regarding the publication of this paper.

References

1. S. Elaydi, R. Lozi, Global dynamics of discrete mathematical models of tuberculosis, *J. Biol. Dynam.*, **18** (2024), 2323724. https://doi.org/10.1080/17513758.2024.2323724
2. S. Mandal, P. Biswas, W. Ansar, P. Mukherjee, J. J. Jawed, *Tuberculosis of the central nervous system: Pathogenicity and molecular mechanism*, In: A Review on Diverse Neurological Disorders, Elsevier, 2024, 93–102. https://doi.org/10.1016/B978-0-323-95735-9.00050-4
3. X. He, Threshold dynamics for a tuberculosis model with seasonality, *Math. Biosci. Eng.*, **9** (2011), 111–122. https://doi.org/10.3934/mbe.2011.9.111
4. M. Shah, S. E. Dorman, Latent tuberculosis infection, *New Engl. J. Med.*, **385** (2021), 2271–2280. https://doi.org/10.1056/NEJMra2039400
5. M. Adhikari, Tuberculosis and tuberculosis/HIV co-infection in pregnancy, *Semin. Fetal Neonat. M.*, **14** (2009), 234–240. https://doi.org/10.1016/j.siny.2009.02.001

6. P. E. M. Fine, BCG vaccination against tuberculosis and leprosy, *Brit. Med. Bull.*, **44** (1988), 691–703.
7. A. Roy, M. Eisenhut, R. J. Harris, L. C. Rodrigues, S. Sridhar, S. Habermann, et al., Effect of BCG vaccination against Mycobacterium tuberculosis infection in children, *BMJ*, **349** (2014), g4643. https://doi.org/10.1136/bmj.g4643
8. M. Igoe, R. Casagrandi, M. Gatto, C. M. Hoover, L. Mari, C. N. Ngonghala, et al., Reframing optimal control problems for infectious disease management in low-income countries, *Bull. Math. Biol.*, **85** (2023), 31. https://doi.org/10.1007/s11538-023-01112-5
9. J. I. Irunde, J. Z. Ndendya, J. A. Mwasunda, P. K. Robert, Modeling the impact of screening and treatment on typhoid fever dynamics in unprotected population, *Results Phys.*, **50** (2023), 107120. https://doi.org/10.1016/j.rinp.2023.107120
10. M. De la Sen, S. Alonso-Quesada, A. Ibeas, On the stability of an SEIR epidemic model with distributed time-delay and a general class of feedback vaccination rules, *Appl. Math. Comput.*, **268** (2015), 639–654. https://doi.org/10.1016/j.amc.2015.08.099
11. C. Ozcaglar, A. Shabbeer, S. L. Vandenberg, B. Yener, K. P. Bennett, Epidemiological models of Mycobacterium tuberculosis complex infections, *Math. Biosci.*, **236** (2012), 77–96. https://doi.org/10.1016/j.mbs.2012.02.003
12. M. S. Abdelouahab, A. Arama, R. Lozi, Bifurcation analysis of a model of tuberculosis epidemic with treatment of wider population suggesting a possible role in the seasonality of this disease, *Chaos*, **31** (2021), 123125. https://doi.org/10.1063/5.0057635
13. F. O. Ochieng, SEIRS model for TB transmission dynamics incorporating the environment and optimal control, *BMC Infect. Dis.*, **25** (2025), 490. https://doi.org/10.1186/s12879-025-10710-2
14. L. Liu, X. Q. Zhao, Y. Zhou, A tuberculosis model with seasonality, *Bull. Math. Biol.*, **72** (2010), 931–952. https://doi.org/10.1007/s11538-009-9490-3
15. J. M. Trauer, J. T. Denholm, E. S. McBryde, Construction of a mathematical model for tuberculosis transmission, *J. Theor. Biol.*, **358** (2014), 74–84.
16. R. S. Wallis, Mathematical models of tuberculosis reactivation and relapse, *Front. Microbiol.*, **7** (2016), 669. https://doi.org/10.3389/fmicb.2016.00669
17. J. Zhang, Y. Li, X. Zhang, Mathematical modeling of tuberculosis data of China, *J. Theor. Biol.*, **365** (2015), 159–163.
18. B. Chennaf, M. S. Abdelouahab, R. Lozi, Analysis of the dynamics of tuberculosis in Algeria, *Computation*, **11** (2023), 146. https://doi.org/10.3390/computation11030146
19. B. Chennaf, M. S. Abdelouahab, R. Lozi, A novel compartmental VSLIT model for TB in Algeria and Ukraine, *Ukr. Math. J.*, **75** (2023), 1709–1722.
20. R. Boucherma, M. S. Abdelouahab, R. Lozi, A fractional-order VSEITR model with Caputo derivative for analyzing tuberculosis dynamics and control strategies in Algeria, *J. Appl. Nonlinear Dyn.*, 2026, in press.
21. B. Chennaf, M. S. Abdelouahab, Discrete-time epidemic modeling with chemoprophylaxis, *J. Innov. Appl. Math. Comput. Sci.*, **4** (2024), 63–85.

22. H. Joshi, M. Yavuz, Fractional-order COVID-19 and TB coinfection model, *Eur. Phys. J. Plus*, **138** (2023), 468. https://doi.org/10.1140/epjp/s13360-023-03916-x
23. O. J. Peter, A. Abidemi, F. Fatmawati, M. M. Ojo, F. A. Oguntolu, Optimizing tuberculosis control: A comprehensive simulation of integrated interventions using a mathematical model, *Math. Model. Numer. Simul. Appl.*, **4** (2024), 238–255.
24. W. Ahmad, A. I. K. Butt, M. Rafiq, Z. Asif, T. Ismaeel, N. Ahmad, Modeling, analyzing and simulating the measles transmission dynamics through efficient computational optimal control technique, *Eur. Phys. J. Plus*, **139** (2024), 345. https://doi.org/10.1140/epjp/s13360-024-0345-0
25. M. Yavuz, M. Akman, F. Usta, N. Özdemir, Effect of awareness in a fractional TB model, *AIP Conf. Proc.*, **2483** (2022), 010001. https://doi.org/10.1063/5.0094321
26. B. Bolaji, T. Onoja, A. C. Benedict, B. I. Omede, U. B. Odionyenma, Dynamical analysis of HIV-TB co-infection transmission model in the presence of treatment for TB, *Bull. Biomath.*, **2** (2024), 21–56.
27. M. Yavuz, F. Özköse, M. Akman, Z. T. Taştan, TB epidemic under consciousness effect, *Math. Model. Control*, **3** (2023), 88–103.
28. Attaullah, K. Mahdi, M. Yavuz, S. Boulaaras, M. Haiour, V. T. Pham, Computational approaches on integrating vaccination and treatment strategies in the SIR model using Galerkin time discretization scheme, *Math. Comput. Model. Dyn. Syst.*, **30** (2024), 758–791. https://doi.org/10.1080/13873954.2024.2405504
29. L. Boulaasair, H. Bouzahir, M. Yavuz, Global analysis of a patchy epidemic model, *Int. J. Optim. Control*, **14** (2024), 365–377.
30. M. Yavuz, K. Akyüz, N. B. Bayraktar, F. N. Özdemir, Fractional hepatitis-B modeling with real data, *AIMS Biophys.*, **11** (2024), 378–402.
31. T. R. Nandi, A. K. Saha, S. Roy, Fractional-order TB model with vaccination and reinfection, *Sci. Rep.*, **14** (2024), 28290. https://doi.org/10.1038/s41598-024-56345-7
32. *World Health Organization*, Algeria factsheets of health statistics 2010, 2022. Available from: `https://www.afro.who.int/fr/node/5820`.
33. *World Bank Group*, Tuberculosis treatment success rate, Algeria, 2022. Available from: `https://data.worldbank.org/indicator/SH.TBS.CURE.ZS?locations=DZ`.
34. J. Ripoll, J. Font, A discrete model for the evolution of infection prior to symptom onset, *Mathematics*, **11** (2023), 1092. https://doi.org/10.3390/math11051092
35. E. W. Tiemersma, M. J. van der Werf, M. W. Borgdorff, B. G. Williams, C. Dye, Natural history of tuberculosis: Duration and fatality of untreated pulmonary tuberculosis in HIV negative patients, *PLoS One*, **6** (2011), e17601. https://doi.org/10.1371/journal.pone.0017601
36. O. Diekmann, J. A. P. Heesterbeek, J. A. J. Metz, On the definition and the computation of the basic reproduction ratio R_0 in models for infectious diseases in heterogeneous populations, *J. Math. Biol.*, **28** (1990), 365–382.
37. P. van den Driessche, J. Watmough, Reproduction numbers and sub-threshold endemic equilibria for compartmental models of disease transmission, *Math. Biosci.*, **180** (2002), 29–48.

38. J. P. LaSalle, Some extensions of Liapunov's second method, *IRE T. Circ. Theor.*, **7** (1960), 520–527. https://doi.org/10.1109/TCT.1960.1086720

39. *World Health Organization*, Global tuberculosis report, 2022. Available from: `https://extranet.who.int/tme/generateCSV.asp?ds=notifications`.

40. *Population growth in Algeria*, 2024. Available from: `https://www.donneesmondiales.com/afriquealgerie/croissance-population.php`.

41. I. Abubakar, L. Pimpin, C. A. Ariti, R. Beynon, P. Mangtani, J. A. C. Sterne, et al., Systematic review and meta-analysis of the current evidence on the duration of protection by bacillus Calmette–Guérin vaccination against tuberculosis, *Health Technol. Assess.*, **17** (2013), 1–372. https://doi.org/10.3310/hta17370

42. J. A. C. Sterne, G. Rodrigues, C. A. Glynn, J. F. Watson, A. P. Sutherland, P. Mangtani, Decline of BCG efficacy with time, *Int. J. Tuberc. Lung Dis.*, **2** (1998), 200–207.

43. P. Mangtani, I. Abubakar, C. Ariti, R. Beynon, L. Pimpin, P. E. Fine, et al., Protection by BCG vaccine against tuberculosis: A systematic review of randomized controlled trials, *Clin. Infect. Dis.*, **58** (2014), 470–480. https://doi.org/10.1093/cid/cit790

44. *Trading Economics*, Immunization, BCG, Algeria, 2022. Available from: `https://www.tradingeconomics.com/algeria/immunization-bcg-percent-of-one-year-old-old-children-wb-data.html`.

45. S. Selmane, The impact of treatment of latent tuberculosis on the incidence: The case of Algeria, *Int. J. Math. Comput. Sci.*, **8** (2014), 961–966.

AIMS Press